MBoC | ARTICLE

Regulation of neurofilament length and transport by a dynamic cycle of phospho-dependent polymer severing and annealing

Atsuko Uchida[a,†], Juan Peng[b], and Anthony Brown[a,*]
[a]Department of Neuroscience and [b]Center for Biostatistics and Department of Biomedical Informatics, Ohio State University, Columbus, OH 43210

ABSTRACT **Neurofilaments are cargoes of axonal transport which are unique among known intracellular cargoes in that they are long, flexible protein polymers. These polymers are transported into axons, where they accumulate in large numbers to drive the expansion of axon caliber, which is an important determinant of axonal conduction velocity. We reported previously that neurofilaments can be lengthened by joining ends, called end-to-end annealing, and that they can be shortened by severing. Here, we show that neurofilament annealing and severing are robust and quantifiable phenomena in cultured neurons that act antagonistically to regulate neurofilament length. We show that this in turn regulates neurofilament transport and that severing is regulated by N-terminal phosphorylation of the neurofilament subunit proteins. We propose that focal destabilization of intermediate filaments by site-directed phosphorylation may be a general enzymatic mechanism for severing these cytoskeletal polymers, providing a mechanism to regulate the transport and accumulation of neurofilaments in axons.**

Monitoring Editor
Stephanie Gupton
University of North Carolina at Chapel Hill

Received: Jan 24, 2023
Revised: Mar 17, 2023
Accepted: Mar 22, 2023

INTRODUCTION

Neurofilaments, which are the intermediate filaments of nerve cells, are space-filling polymers that accumulate in axons during development to expand axon caliber and thus increase axonal conduction velocity (Hoffman, 1995; Lariviere and Julien, 2004). These polymers are assembled in the neuronal cell body (Black *et al.*, 1986) and transported into and along axons by the mechanisms of axonal transport (Roy *et al.*, 2000; Wang *et al.*, 2000). Notably, neurofilaments are unique among other known axonally transported cargoes in that they are long flexible protein polymers, measuring just 10 nm in diameter and up to 40 μm or more in length (Yan and Brown, 2005; Fenn *et al.*, 2018a,b). These polymers move bidirectionally along microtubule tracks powered by kinesin and dynein motors (Francis *et al.*, 2005; He *et al.*, 2005; Uchida *et al.*, 2009). The movement is characterized by short bouts of rapid movement interrupted by prolonged pauses, resulting in an overall slow rate of movement (Brown, 2000). Keratin and vimentin filaments have also been reported to move along microtubule tracks, suggesting that such movements are a general property of intermediate filaments (Leduc and Etienne-Manneville, 2017; Robert *et al.*, 2019).

Studies in vitro have shown that intermediate filaments lengthen by joining at their ends, a process known as end-to-end annealing (Herrmann *et al.*, 1999; Wickert *et al.*, 2005; Mucke *et al.*, 2016). Using photobleaching/photoconversion strategies, we demonstrated extensive end-to-end annealing of vimentin filaments and neurofilaments in cell lines (Colakoglu and Brown, 2009) and in primary neurons (Uchida *et al.*, 2013). During those studies, we discovered that neurofilaments can also be severed (Uchida *et al.*, 2013; Fenn *et al.*, 2018a). Subsequently, severing and annealing were reported by others for vimentin filaments (Hookway *et al.*, 2015). End-to-end annealing occurs spontaneously in vitro in the absence of accessory factors (Winheim *et al.*, 2011) and likely involves overlap

This article was published online ahead of print in MBoC in Press (http://www.molbiolcell.org/cgi/doi/10.1091/mbc.E23-01-0024) on March 29, 2023.

Conflict of interest: The authors declare that they have no competing financial interests.

†Present address: Center for Humanities and Sciences, Ibaraki Prefectural University of Health Sciences, 4669-2 Ami, Ami-machi, Inashiki-gun, Ibaraki 300-0394, Japan.

*Address correspondence to: Anthony Brown (brown.2302@osu.edu).

Abbreviations used: cAMP, cyclic adenosine monophosphate; GFP, green fluorescent protein; NFH, neurofilament protein H; NFL, neurofilament protein L; NFM, neurofilament protein M; OA, okadaic acid; PKA, protein kinase A; β, beta coefficient.

or interdigitation of the staggered coiled-coil dimer overhangs at the ends of each intermediate filament (Colakoglu and Brown, 2009; Lopez *et al.*, 2016). However, the mechanism of intermediate filament severing is unknown.

Our discovery that neurofilament length can be altered by severing and annealing has led us to ask whether neurofilament length has any significance for neurofilament function. One possibility is that their length might influence their axonal transport. However, analysis of neurofilament transport on short timescales (seconds or minutes) has revealed no decrease in neurofilament transport velocity with increasing polymer length for filaments ranging from 0.6 to 42 μm in length (Fenn *et al.*, 2018a). Here, we investigate neurofilament transport on longer timescales (tens of minutes) and report an unexpected dependence of neurofilament pausing, reversing, severing, and annealing on neurofilament length. Our data suggest that neurofilament length and transport are regulated by a dynamic cycle of severing and annealing. We show that this cycle is regulated by phosphorylation and that site-directed phosphorylation may be a mechanism for neurofilament severing.

RESULTS

To visualize neurofilaments, we cotransfected dissociated cortical neurons with green fluorescent protein (GFP)-tagged neurofilament protein M (NFM) (GFP-NFM) (Wang and Brown, 2001) and EB3-mCherry (to allow assessment of axon orientation). We then observed the cells after 8–10 d in culture. The GFP fusion protein coassembles fully with endogenous neurofilament proteins, and the low neurofilament content of these neurons makes it possible to track single moving filaments (Uchida *et al.*, 2016). Our previous time-lapse imaging of neurofilament transport was limited to short-term observations because the filaments moved rapidly out of the camera field of view. To overcome this problem, we used the motorized stage on our microscope to recenter the moving filaments when they approached the edge of the field of view, allowing us to record their movement across multiple fields of view (see *Materials and Methods*). We then used the stage position of each frame in the resulting movies to register the images, creating a movie montage (Supplemental Movie S1). Using this multifield time-lapse tracking approach, we were able to follow the movement of single neurofilaments along axons for distances of 0.5 mm or more (Figure 1A).

Dependence of transport kinetics on filament length

To investigate the dependence of neurofilament transport on polymer length, we acquired 76 long-term, multifield time-lapse movies of moving filaments in neonatal rat cortical neurons after 8–10 d in culture. The resulting movies often also captured the movement of other filaments. Thus, during the subsequent analysis, we tracked all filaments in the movies that met our analysis criteria (see *Materials and Methods*). In total, we obtained trajectories for the movement of 93 filaments, which ranged from 1.3 to 48.3 μm in length. Fifty-five moved in a net anterograde direction, and 38 moved in a net retrograde direction.

Figure 1, B–I, shows representative examples of the trajectories of eight filaments, four "short" filaments (2.5–6.9 μm in length) and four "long" filaments (18.9–31.3 μm in length). As we have reported previously, filaments of all lengths moved rapidly on short timescales (seconds to minutes) (Fenn *et al.*, 2018a). However, we observed a marked difference on longer timescales (tens of minutes). Short filaments exhibited a clear directional preference (anterograde or retrograde), and they tended to move persistently in that direction throughout the tracking period, pausing and reversing relatively infrequently. Long filaments were also capable of rapid movement, sometimes for several minutes or more, but they paused more and reversed direction more frequently. As a result, the movement of long filaments often resulted in little net displacement.

To quantify the relationship between transport kinetics and filament length on long timescales, we further analyzed all those filaments that we were able to track for at least 8 min ($n = 65$ filaments). Figure 2 shows scatterplots of net average transport velocity, percent time pausing, directional persistence, and peak velocity versus filament length. Filaments that moved in a net retrograde direction had a 0.138 μm/s greater net average velocity compared with those moved in a net anterograde direction ($p = 0.006$) (Figure 2A). This is consistent with previous reports that neurofilament movement is faster in the retrograde direction than in the anterograde direction (Fenn *et al.*, 2018a). However, for both directions, regression analysis revealed a marked and statistically significant decrease in net average velocity with increasing filament length ($p < 0.0001$). Quantification of the moving and pausing behavior confirmed that this decrease in net average velocity was due to an increase in the time that the filaments spent pausing ($p < 0.0001$) (Figure 2B) and a decrease in their directional persistence, that is, the proportion of the time the filaments spent moving in the direction of their net movement ($p < 0.0001$) (Figure 2C). There was no statistically significant difference in percent time pausing ($p = 0.5$) or directional persistence ($p = 0.15$) with respect to the direction of movement, but the peak velocity was 1.72 μm/s greater in the retrograde direction than in the anterograde direction ($p < 0.0001$). For every 1 μm increase in filament length, we observed a velocity decrease of 0.016 μm/s, a 1.1% increase in percent time pausing and a 1.5% decrease in directional persistence. In contrast, though there was considerable scatter in the data, the absolute peak velocity exhibited no significant length dependence in either direction ($p = 0.32$) (Figure 2D).

Dependence of annealing and severing frequency on filament length

The tracked filaments sometimes exhibited severing or end-to-end annealing. Examples are shown in Figure 3 and Supplemental Movies S2 and S3. To quantify the annealing and severing frequency, we counted the total annealing and severing events in the 76 movies analyzed above. We also included an additional 21 movies that we excluded from the original data set due to ambiguity in the axon orientation or due to the use of time-lapse intervals of 2 s instead of 3 s. In total, we observed 29 severing events and 15 end-to-end annealing events, corresponding to an average filament severing rate of 0.9 events/h and an average filament annealing rate of 0.5 events/h (141 filaments tracked; 32 h total tracking time). Thus, approximately one third of the filaments that we tracked exhibited a severing or annealing event. To investigate the effect of filament length, we analyzed the dependence of these rates on the length of the tracked filament (Figure 3, C and D; Supplemental Movies S4 and S5). Analysis using binary logistic regression revealed that there was a statistically significant difference between the average lengths of filaments that annealed (9.3 ± 7.7 μm, $n = 15$), those that severed (22.1 ± 11.9 μm, $n = 29$), and those that neither annealed nor severed (15.6 ± 12.2 μm, $n = 97$) ($p = 0.0007$). For every 1 μm increase in filament length, the probability of severing increased by 4.7% (95% confidence interval: 1.01–1.08) and the probability of annealing decreased by 7.6% (95% confidence interval: 0.86–0.99). Short filaments (<10 μm) exhibited the highest rate of end-to-end annealing (1.24 events/h) but the lowest rate of severing (0.34 events/h). In contrast, long filaments (>20 μm) exhibited the lowest rate of annealing (0.15 events/h) and the highest rate of severing

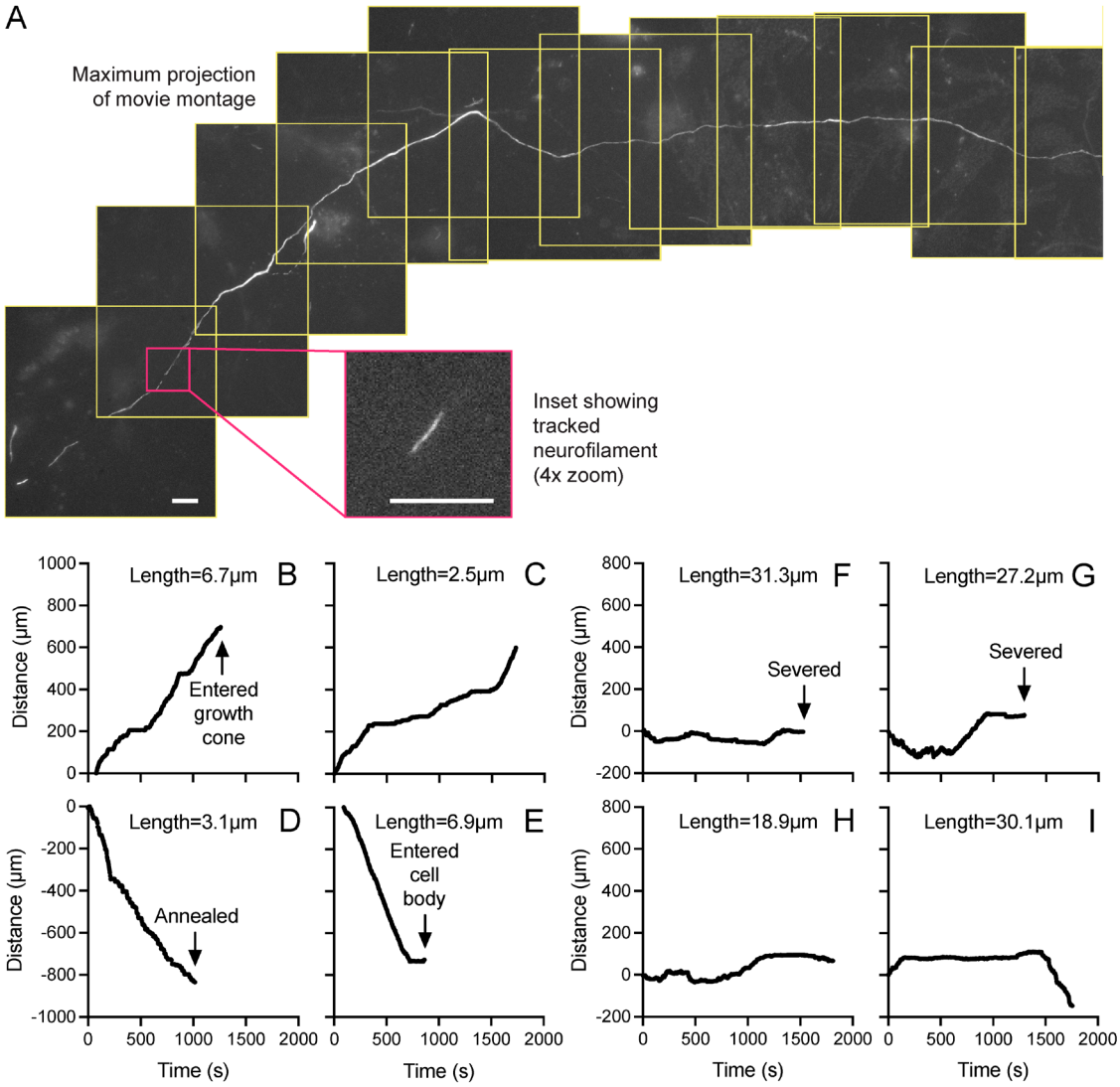

FIGURE 1: Long-range multifield tracking of neurofilaments. (A) Maximum-intensity projection of a multifield time-lapse movie showing the trajectory of a neurofilament along an axon of a neonatal rat cortical neuron after 8 d in culture. The microscope stage was moved 10 times during the movie, allowing the moving filament to be tracked for ~420 µm over a period of 12.4 min (248 images acquired at 3 s time intervals). The images were aligned using the encoded microscope stage coordinates to create a movie montage made up of 11 distinct overlapping fields (yellow boxes). The inset is a region of one image plane at 4× zoom, showing the tracked filament at higher magnification. Scale bar = 10 µm in main figure and inset. (B–E) Representative trajectories of four short filaments (<10 µm in length). (F–I) Representative trajectories of four long filaments (>15 µm in length). Data from multifield time-lapse movies of neonatal rat cortical neurons after 8–10 d in culture. Distance along the axon is plotted vs. time. Anterograde is positive, and retrograde is negative. Each filament was tracked for up to 1800 s (30 min). The tracking was terminated early if the filament reached one end of the axon (B and E), annealed with another filament (D), or severed (F and G). Note that the short filaments moved rapidly and persistently in the anterograde or retrograde direction, whereas the long filaments also moved rapidly, but paused and reversed direction more frequently.

(1.5 events/h). Thus, the rates of severing and end-to-end annealing exhibited inverse length dependencies.

Phosphomimetic and phosphodeficient NFL mutants have different effects on neurofilament length, transport, severing, and annealing

It is known that the intermediate filament protein head domains regulate filament assembly (Gill *et al.*, 1990), and phosphorylation of these domains induces intermediate filament fragmentation and disassembly in vitro and in vivo in a variety of cell types (Inagaki *et al.*, 1987; Ando *et al.*, 1989; Hisanaga *et al.*, 1990; Klymkowsky *et al.*, 1991; Chou *et al.*, 1996; Eriksson *et al.*, 2004; Izawa and Inagaki, 2006). Thus, phosphorylation of the N-terminal head domains of the neurofilament subunit proteins at loci along neurofilament polymers could be a mechanism for neurofilament severing. To test this hypothesis, we obtained a panel of rat neurofilament protein L (NFL) constructs from Chris Miller (King's College, University of London) in which the four serines in the NFL head domain that have been proposed to be phosphorylated in neurons (serines 2, 55, 57, and 62) were mutated to either aspartate or alanine (Yates *et al.*, 2009). Serines 2, 55, and 62 have been reported to be phosphorylated by protein kinase A (PKA) (Sihag and Nixon, 1991; Giasson *et al.*, 1996;

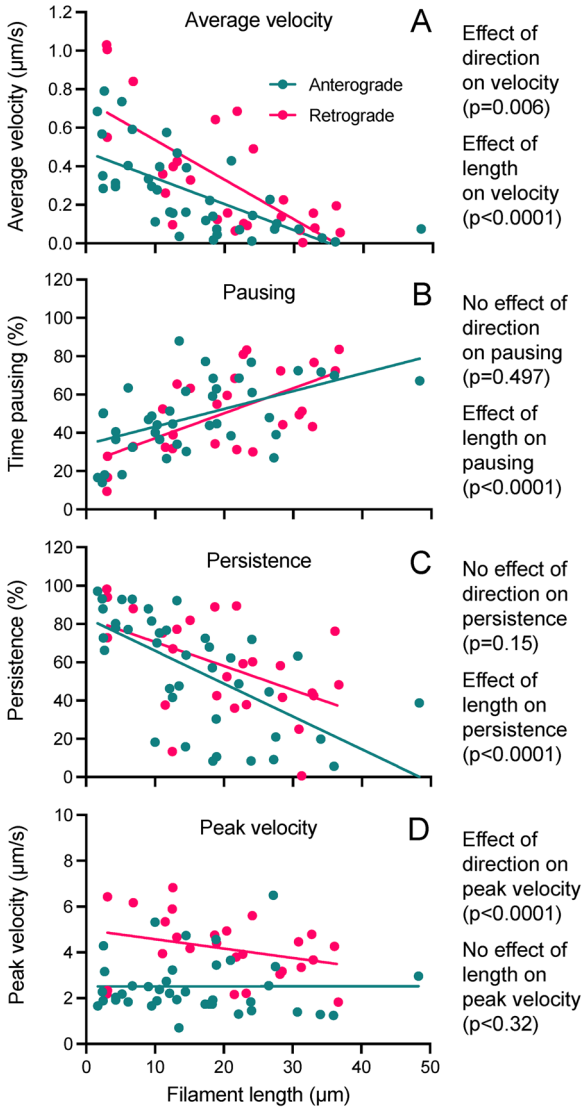

FIGURE 2: Length dependence of neurofilament transport. Scatterplots of the kinetic parameters of neurofilament transport vs. filament length for 65 filaments that were tracked for at least 8 min and up to 30 min each in multifield time-lapse movies of neonatal rat cortical neurons after 8–10 d in culture. (A) Average velocity, which is the net distance moved divided by the duration that the filament was tracked. There was a statistically significant effect of direction ($\beta = -0.17$, SE = 0.05, $p = 0.006$) and length ($\beta = -0.018$, SE = 0.0025, $p < 0.0001$) on velocity (model $R^2 = 0.40$). (B) Percent time pausing. There was a statistically significant effect of length ($\beta = 1.07$, SE = 0.19, $p < 0.0001$) but not direction ($\beta = 2.88$, SE = 4.21, $p = 0.497$) on pausing (model $R^2 = 0.33$). (C) Directional persistence, which is the net distance moved divided by the total distance moved (irrespective of direction). There was a statistically significant effect of length ($\beta = -1.54$, SE = 0.27, $p < 0.0001$) but not direction ($\beta = -8.47$, SE = 5.84, $p = 0.15$) on persistence (model $R^2 = 0.35$). (D) Peak velocity, which is the maximum time-lapse interval velocity for each filament. There was a statistically significant difference in the peak velocity of anterograde and retrograde filaments ($\beta = -1.72$, SE = 0.33, $p < 0.0001$), but there was no dependence of peak velocity on filament length in either the anterograde direction ($\beta = 0.00017$, SE = 0.020, $p = 0.99$) or the retrograde direction ($\beta = -0.041$, SE = 0.025, $p = 0.11$) (model $R^2 = 0.30$). The statistical analysis was performed using a linear regression model for filaments that moved in a net anterograde (teal) or retrograde (magenta) direction. Note that the average net velocity declined with increasing neurofilament length for filaments that moved in either net direction, and this was due to an increase in the percent time pausing and a decrease in the directional persistence of the movement.

Cleverley *et al.*, 1998; Nakamura *et al.*, 2000; Trimpin *et al.*, 2004) and serine 57 by rho kinase and calcium-calmodulin–dependent kinase (CaMKII) (Hashimoto *et al.*, 1998, 2000).

Both the NFL^{S2,55,57,66A} (phosphodeficient) and NFL^{S2,55,57,66D} (phosphomimetic) mutants coassembled with NFM in SW13vim- cells, though the filaments containing the phosphomimetic mutant tended to be shorter (Supplemental Figure S1). To investigate the effect of NFL phosphorylation on neurofilaments in neurons, we expressed fluorescence fusions of these mutants and of wild-type NFL (NFL^{S2,55,57,66A}-GFP, NFL^{S2,55,57,66D}-GFP, or NFL-GFP, respectively) in cultured neonatal rat cortical neurons. In comparison to GFP-NFM, transfection with NFL-GFP alone tended to result in elevated diffuse fluorescence, which is indicative of incomplete incorporation into filaments. We found that this could be avoided by cotransfecting the NFL-GFP fusions with untagged NFM. Under these conditions, both the NFL^{S2,55,57,66A}-GFP and NFL^{S2,55,57,66D}-GFP constructs incorporated fully into neurofilament polymers throughout the cells (Figure 4). In contrast to Yates *et al.* (2009), we did not observe any tendency for the NFL^{S2,55,57,66D} mutant to aggregate.

First, we investigated the neurofilament length distribution and transport frequency in fixed-field time-lapse movies of neurons expressing wild-type NFL-GFP, NFL^{S2,55,57,66D}-GFP (phosphomimetic mutant), or NFL^{S2,55,57,66A}-GFP (phosphodeficient mutant) (Figure 5, A–D; Supplemental Movies S6, S7 and S8). We observed statistically significant interactions for both length and frequency with respect to age in culture ($p < 0.0001$), which is indicative of different change patterns among the three groups. For neurons expressing wild-type NFL, the average filament length increased with age in culture from 6.3 μm at 8 d to 9.2 μm at 11 d, and the average frequency decreased from 7.9 filaments/axon/h at 8 d to 2.3 filaments/axon/h at 11 d. Thus, neurofilaments became longer and less mobile as these neurons matured. Filaments containing phosphomimetic NFL were shorter and increased only slightly in length, from 5.1 μm at 8 d to 5.8 μm at 11 d ($p = 0.023$). However, the frequency of movement of these filaments was similar to that of the wild type, decreasing from 8.2 filaments/axon/h at 8 d to 4.6 filaments/axon/h at 10 d ($p < 0.0001$). In contrast, filaments containing phosphodeficient NFL decreased in length from 13.5 μm at 8 d to 9.1 μm at 10 d ($p = 0.0042$) and then increasing slightly to 9.7 μm at 11 d, though this was not statistically significant ($p = 0.08$). The frequency of movement of these filaments was significantly lower than for filaments containing wild-type and phosphomimetic NFL ($p < 0.0001$) but also decreased over time from 3.1 filaments/axon/h at 8 d to 2.1 filaments/axon/h at 10 d ($p = 0.016$). The explanation for the decrease in the average filament length in cells expressing phospho-deficient NFL is unclear. One possibility is that the expression level of the exogenous protein may decline with time in these transiently transfected cells, diluting its effect over time. It is also possible that phosphorylation of the endogenous NFL in these neurons could increase over time, effectively masking the effect of the exogenous phosphodeficient NFL. Interestingly, we also observed that in older cultures (after 16–21 d in vitro), the neurofilament content was higher in axons expressing phosphodeficient NFL^{S2,55,57,66A}-GFP than in axons expressing phosphomimetic NFL^{S2,55,57,66D}-GFP, resulting in a significant increase in axon width (Figure 5, E and F). This suggests that phosphorylation of these sites regulates neurofilament length, which in turn

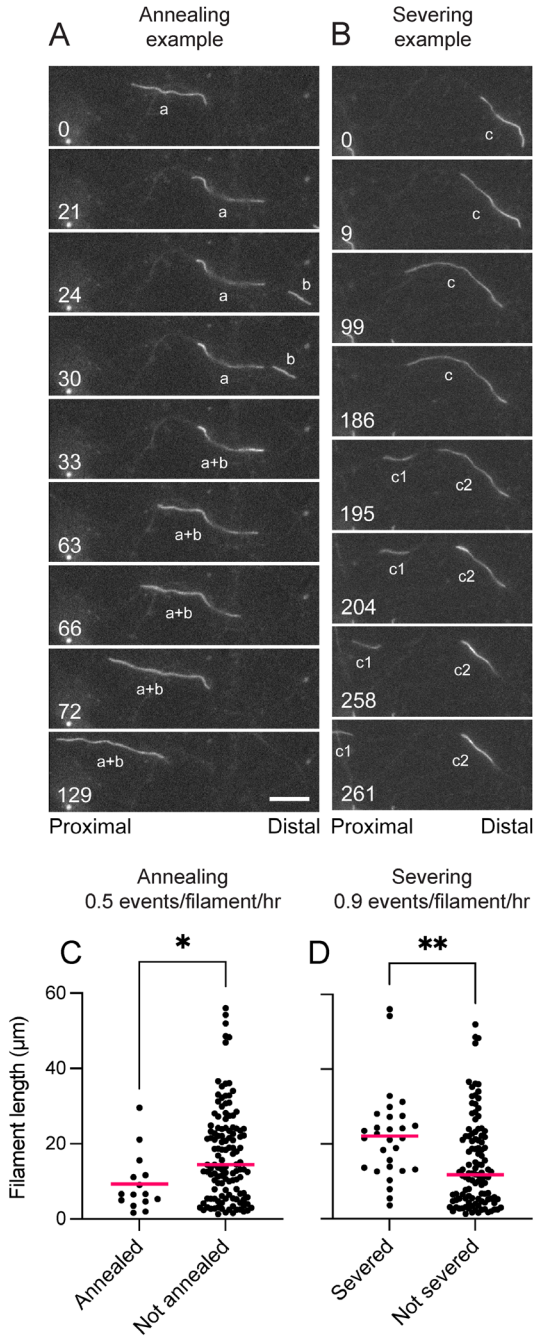

FIGURE 3: Length dependence of neurofilament severing and annealing. (A, B) Excerpts from multifield time-lapse movies of an annealing and a severing event (see Supplemental Movies S2 and S3). Time is shown in seconds. In A, filament "a" (20.8 μm) moved anterogradely (t = 0–21 s) and then paused and folded along part of its length, resulting in an increase in brightness at its proximal end. Note that a portion of this filament passed slightly out of the plane of focus. Filament "b" (6.3 μm) then moved retrogradely into the field of view from the right and overlapped filament "a" (t = 33 s). The two filaments subsequently annealed, and the daughter filament (27.5 μm) moved retrogradely, stretching out as it did so (t = 63–129 s). In B, filament "c" (29 μm) was initially paused and partially folded (t = 0 s) and then stretched out as it moved retrogradely (t = 9–99 s). The filament paused (t = 99–186 s) before severing (t = 195 s). The leading filament fragment ("c1"; 7.1 μm) continued to move retrogradely, and the trailing fragment ("c2"; 21.6 μm) folded back on itself (note the increase in brightness in the folded region) and remained paused. Scale bar = 10 μm. (C, D) Dot plots of filament length for filaments that either annealed or did not anneal and that either severed or did not sever, during the period of observation. Data from 97 movies (141 neurofilaments observed for 32 h; average movie duration = 13.6 min). In all cases, filament length was measured before the severing or annealing event. For the annealing events, we plot the length of the tracked filament. Comparison of the lengths of these tracked filaments (mean = 9.3 ± 7.7 μm; median = 6.6; interquartile range = 7) to those of the untracked filaments with which they annealed (mean = 7.0 ± 5.3 μm; median = 5.9; interquartile range = 6.9) revealed no significant difference (Mann–Whitney U test, p = 0.372). Note that short filaments annealed more frequently than long filaments and that long filaments severed more frequently than short filaments (p = 0.024 in C; p = 0.0057 in D). The statistical analysis was performed using a logistic regression model. The horizontal magenta lines represent the population means. ns ($p > 0.05$), * ($p \leq 0.05$), ** ($p \leq 0.01$).

regulates neurofilament transport and accumulation during axonal maturation.

To investigate the mechanism by which NFL phosphorylation influences neurofilament length, we acquired multifield time-lapse movies and quantified the frequency of neurofilament severing and annealing (Figure 6). Filaments containing phosphodeficient or phosphomimetic NFL exhibited length-dependent severing and annealing as described above (Figure 6, A–D), and the magnitude of this dependence was not significantly different between the two mutants (p = 0.16 for severing and p = 0.23 for annealing). For every micrometer increase in length, the probability of severing increased by 3.4% (95% confidence interval: 1.01–1.06, p = 0.0063) and the probability of annealing decreased by 4.5% (95% confidence interval: 0.92–0.99, p = 0.012). The probability of annealing was also not significantly different between phosphodeficient NFL (average frequency = 0.74 events/filament/h, n = 122 filaments) and phosphomimetic NFL (average frequency = 0.76 events/filament/h, n = 122 filaments) (p = 0.41). However, the probability of severing was 90% less for phosphodeficient NFL (average frequency = 0.16 events/filament/h, n = 122 filaments) compared with phosphomimetic NFL (average frequency = 1.23 events/filament/h, n = 122 filaments) (95% confidence interval: 0.03–0.28, $p < 0.0001$) (Figure 6E). The lack of a significant difference in the annealing frequencies for the phosphodeficient and phosphomimetic NFL mutants may reflect the fact that annealing requires an encounter between two filament ends, which is dependent on the frequency of movement. Thus, it is possible that any decrease in the tendency of filaments containing phosphomimetic NFL to anneal could be masked by an increased in their frequency of movement, which would result in an increase in end-to-end encounters. Nevertheless, our data are consistent with the hypothesis that NFL phosphorylation favors neurofilament severing.

Our interpretation of the neurofilament transport data in Figure 5 is that neurofilament phosphorylation affects neurofilament length, which in turn affects neurofilament transport. However, it is also theoretically possible that phosphorylation somehow affects neurofilament transport, which in turn somehow affects neurofilament length. To test this, we tracked the filaments containing phosphodeficient and phosphomimetic mutant NFL in the multifield time-lapse movies. The dependencies of the average velocity on filament length in both net anterograde and net retrograde directions were similar for the two mutants (Figure 6, F and G). In other words, filaments containing phosphodeficient NFL moved with a velocity similar to that of filaments of comparable length containing phosphomimetic NFL. Thus, the different effects of the NFL mutants on neurofilament transport were due at least primarily to the effect of these mutants on neurofilament length.

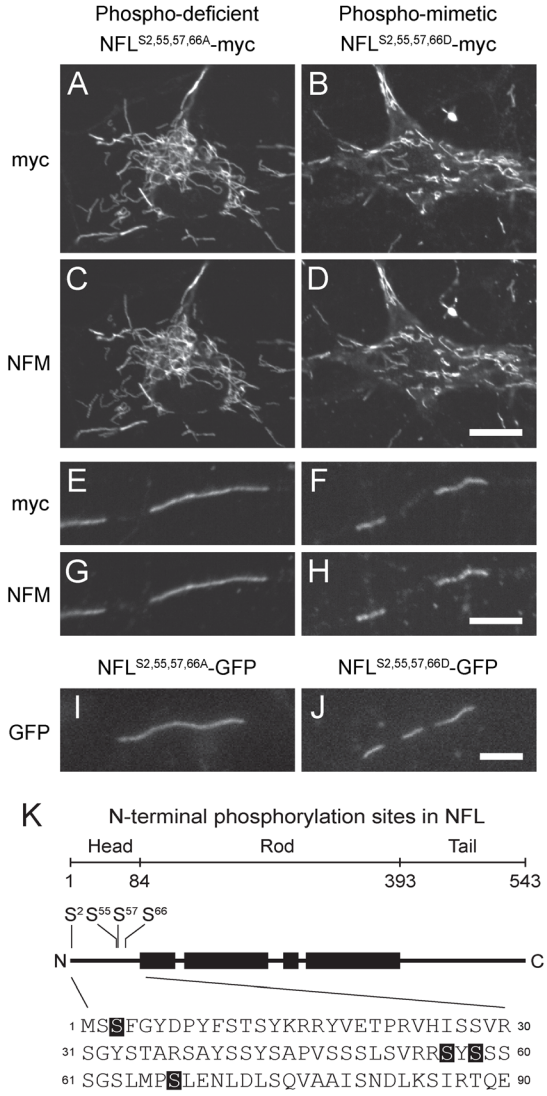

FIGURE 4: Phosphomimetic and phosphodeficient mutant NFL assembles into neurofilaments. (A–H) Spinning-disk confocal microscopy of neurofilaments in cell bodies (A–D) and axons (E–H) of neonatal rat cortical neurons expressing NFL^{S2,55,57,66A}-myc (phosphodeficient mutant) or NFL^{S2,55,57,66D}-myc (phosphomimetic mutant) 10–11 d after plating, immunostained for myc and NFM. The colocalization of myc and NFM confirms that the mutant NFL coassembled into neurofilaments with NFM. (I, J) Live wide-field imaging of axonal neurofilaments in axons of neurons expressing NFL^{S2,55,57,66A}-GFP or NFL^{S2,55,57,66D}-GFP 10 d after plating. Note the uniform incorporation of the mutant proteins along the neurofilaments and the absence of aggregates or diffuse fluorescence, which confirms that the mutant proteins assemble fully into neurofilaments. On average, the neurofilaments containing phosphomimetic NFL were shorter, which is confirmed by the quantitative analysis in Figure 6. Scale bars = 5 μm. (K) Schematic showing the location of the mutated serine residues in the N-terminal head domain of the NFL protein. Note that the numbering of the residues ignores the N-terminal methionine (see explanation in *Materials and Methods*).

Activators of protein kinase A reduce neurofilament length

Three of the four sites mutated in the phosphomimetic and phosphodeficient NFL constructs used above are substrates for PKA (Sihag and Nixon, 1990, 1991; Sihag *et al.*, 2007; Hisanaga *et al.*, 1994; Giasson *et al.*, 1996; Giasson and Mushynski, 1998; Cleverley *et al.*, 1998; Nakamura *et al.*, 2000). Phosphorylation by PKA in vitro causes local thinning and fragmentation of NFL homopolymers and native neurofilaments at sites along their length (Hisanaga *et al.*, 1994) and also arrests the assembly NFL homopolymers at the octamer stage (Hisanaga *et al.*, 1990). The neurofilament head domains can also be dephosphorylated by protein phosphatases 1 and 2A (PP1 and PP2A, respectively) (Sacher *et al.*, 1994; Strack *et al.*, 1997). PP2A dephosphorylates neurofilament proteins that have been phosphorylated by PKA and renders them competent to assemble (Saito *et al.*, 1995; Giasson *et al.*, 1996). Okadaic acid (OA), which is a selective inhibitor of PP1 and PP2A, increases neurofilament head domain phosphorylation and induces reversible neurofilament fragmentation and disassembly in cultured neurons (Sacher *et al.*, 1992, 1994; Giasson *et al.*, 1996; Giasson and Mushynski, 1998). This effect is thought to be due primarily to PP2A inhibition (Sacher *et al.*, 1994) and is potentiated by PKA activation (Giasson *et al.*, 1996). Collectively, these findings demonstrate that the structural integrity of neurofilaments is regulated by phosphorylation and dephosphorylation of the neurofilament protein head domains, particularly by the antagonistic effects of PKA and PP2A. Thus, we hypothesized that phosphorylation by PKA is a potential mechanism for neurofilament severing in axons.

To test whether PKA regulates neurofilament length in neurons, we treated cultured neonatal rat cortical neurons expressing wild-type or phosphodeficient NFL^{S2,55,57,66A}-GFP with 2 mM 8-bromoadenosine 3′,5′-cyclic monophosphate (8-Br-cAMP), which is a membrane-permeant activator of PKA, and/or 5 nM OA after 9 d in culture. We then measured the lengths of moving neurofilaments in fixed-field time-lapse movies as described above (Figure 7). The average filament length was 10.7 ± 9.2 μm in untreated neurons expressing NFL-GFP (Figure 7A). 8-Br-cAMP reduced the average length to 9.1 ± 7.6 μm ($p = 0.0085$). The average filament length in neurons treated with OA was 8.1 ± 6.5 μm, but this was not significantly different from the untreated control ($p = 0.057$). However, a combination of OA plus 8-Br-cAMP reduced the average length to 5.0 ± 3.7 μm ($p < 0.0001$). To test whether this effect was due to a direct action on neurofilaments, we repeated these experiments with neurons expressing NFL^{S2,55,57,66A}-GFP, which is not phosphorylatable at these four sites (Figure 7B). The average filament length was 12.9 ± 11.2 μm. As expected, this was significantly greater than in neurons expressing NFL-GFP ($p = 0.0001$). 8-Br-cAMP reduced the average length to 10.4 ± 8.3 μm ($p = 0.037$). The average filament length in neurons treated with OA was 12.6 ± 8.1 μm, which was not significantly different from that of the untreated control ($p = 0.56$). A combination of OA plus 8-Br-cAMP reduced the average length to 8.2 ± 7.6 μm ($p < 0.0001$), but the magnitude of this reduction was less than for GFP-NFL ($p < 0.0001$). Thus, transfection of the neurons with phosphodeficient NFL^{S2,55,57,66A}-GFP partially protected the neurofilaments from the effects of PKA activation.

A possible explanation for why phosphodeficient NFL^{S2,55,57,66A}-GFP offered only partial protection against activators of PKA is that the cells expressed endogenous phosphorylatable NFL in addition to the exogenous mutant NFL. To address this, we repeated the experiment in cortical neurons from neonatal NFL$^{-/-}$ knockout mice using mouse constructs of NFL-GFP and NFL^{S2,55,57,66A}-GFP. As expected, the average filament length was greater (11.8 ± 8.6 μm) in neurons expressing phosphodeficient NFL^{S2,55,57,66A}-GFP than in neurons expressing NFL-GFP (9.3 ± 7.2 μm) and this difference was statistically significant ($p < 0.0001$). In addition, the protective effect of this mutant was much more pronounced. Treatment of cortical neurons expressing NFL-GFP with 8-Br-cAMP plus OA reduced the average filament length from 9.3 ± 7.2 μm to 3.6 ± 3.4 μm ($p < 0.0001$) (Figure 7C; Supplemental Movie S9). In contrast, the same

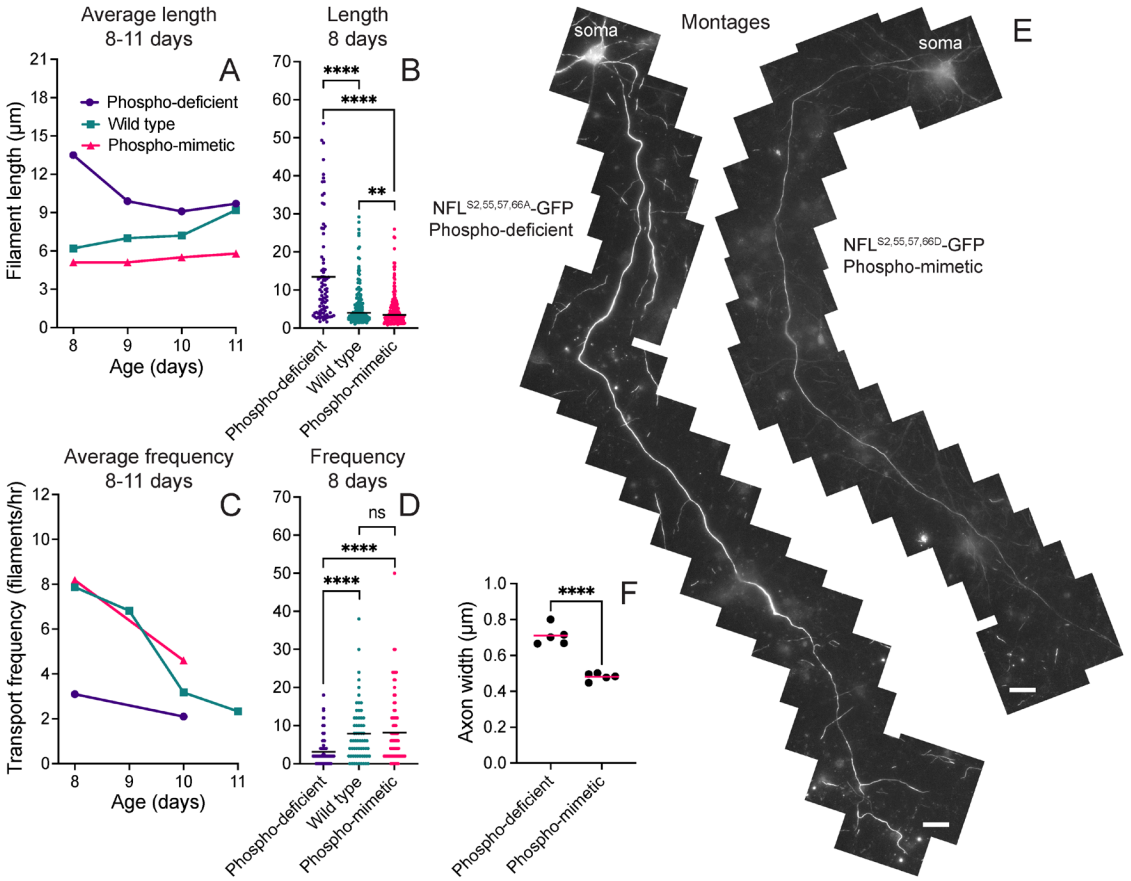

FIGURE 5: Phosphomimetic and phosphodeficient NFL mutants influence neurofilament length, transport frequency, and accumulation. Neonatal rat cortical neurons expressing either wild-type NFL-GFP, NFL^{S2,55,57,66A}-GFP (phosphodeficient mutant), or NFL^{S2,55,57,66D}-GFP (phosphomimetic mutant). (A) Average neurofilament length vs. age in culture. Each data point represents the average of 87–253 filaments (average = 163) measured in four to nine fixed-field time-lapse movies (average = 5.9) of 15 min duration. (B) Dot plot of neurofilament lengths at 8 d. We measured 87 filaments in five movies for phosphodeficient NFL, 143 filaments in five movies for the wild type, and 146 filaments in five movies for phosphomimetic NFL. (C) Average neurofilament transport frequency vs. age in culture. Each data point represents the average of 28–360 filaments (average = 144) measured in 21–88 axons (average = 52) in 3–14 fixed-field time-lapse movies (average = 8) of 30 min duration. (D) Dot plot of neurofilament transport frequencies at 8 d. We measured 131 filaments in 86 axons in 10 movies for phosphodeficient NFL, 248 filaments in 63 axons in 13 movies for the wild type, and 360 filaments in 88 axons in 11 movies for phosphomimetic NFL. The horizontal black lines represent the population means. Note that in A–D there is an age-dependent increase in filament length accompanied by an age-dependent decrease in transport frequency in neurons expressing wild-type NFL-GFP but at all ages the filaments were longer and moved less frequently in neurons expressing phosphodeficient NFL and were shorter in neurons expressing phosphomimetic NFL. For phosphodeficient NFL, filament length was significantly lower on day 10 compared with day 8 ($p = 0.0042$) but was not significantly different between day 8 and day 9 ($p = 0.10$) or between day 8 and day 11 ($p = 0.08$). For phosphomimetic NFL, filament lengths on day 10 ($p = 0.041$) and day 11 ($p = 0.023$) were significantly greater than on day 8. For the wild type, filament length was significantly greater on day 11 compared with days 8 ($p < 0.0001$), 9 ($p = 0.05$), and 10 ($p = 0.0034$). Filaments containing phosphodeficient NFL were significantly longer than filaments containing phosphomimetic NFL on days 8 ($p < 0.0001$), 9 ($p < 0.0001$), 10 ($p < 0.0001$), and 11 ($p < 0.0001$). Filaments containing phosphodeficient NFL were significantly longer than filaments containing the wild type on days 8 ($p < 0.0001$), 9 ($p = 0.0047$), and 10 ($p = 0.0034$), but not on day 11 ($p = 0.1$). Filaments containing phosphomimetic NFL were significantly shorter than for the wild type on days 8 ($p = 0.01$), 9 ($p < 0.0001$), 10 ($p = 0.0061$), and 11 ($p < 0.0001$). For the transport frequency, the wild type decreased more from 8 to 10 d than either of the mutants ($p < 0.0001$). The frequency at 8 d was significantly higher for the wild-type and phosphomimetic NFL compared with phosphodeficient NFL ($p < 0.0001$). The frequency at 10 d was significantly higher for phosphomimetic NFL compared with the wild-type and phosphodeficient NFL ($p < 0.0001$). The statistical analysis was performed using a linear regression model in A and B and a Poisson regression model in C and D. (E) Montages of axons of cortical neurons transfected with phosphodeficient NFL^{S2,55,57,66A}-GFP or phosphomimetic NFL^{S2,55,57,66D}-GFP and then imaged live 16–21 d later using the spinning-disk confocal microscope in wide-field bypass mode. Scale bars = 25 μm. (F) Average axon width for axons expressing the NFL^{S2,55,57,66A}-GFP phosphodeficient mutant ($n = 5$) or the NFL^{S2,55,57,66D}-GFP phosphomimetic mutant ($n = 5$). The data were compared using an unpaired t test for equal variances ($p < 0.0001$). The horizontal magenta lines represent the population means. Note that the axon expressing phosphodeficient NFL is brighter and wider, indicating a higher neurofilament content. ns ($p > 0.05$), ** ($p \leq 0.01$), **** ($p \leq 0.0001$).

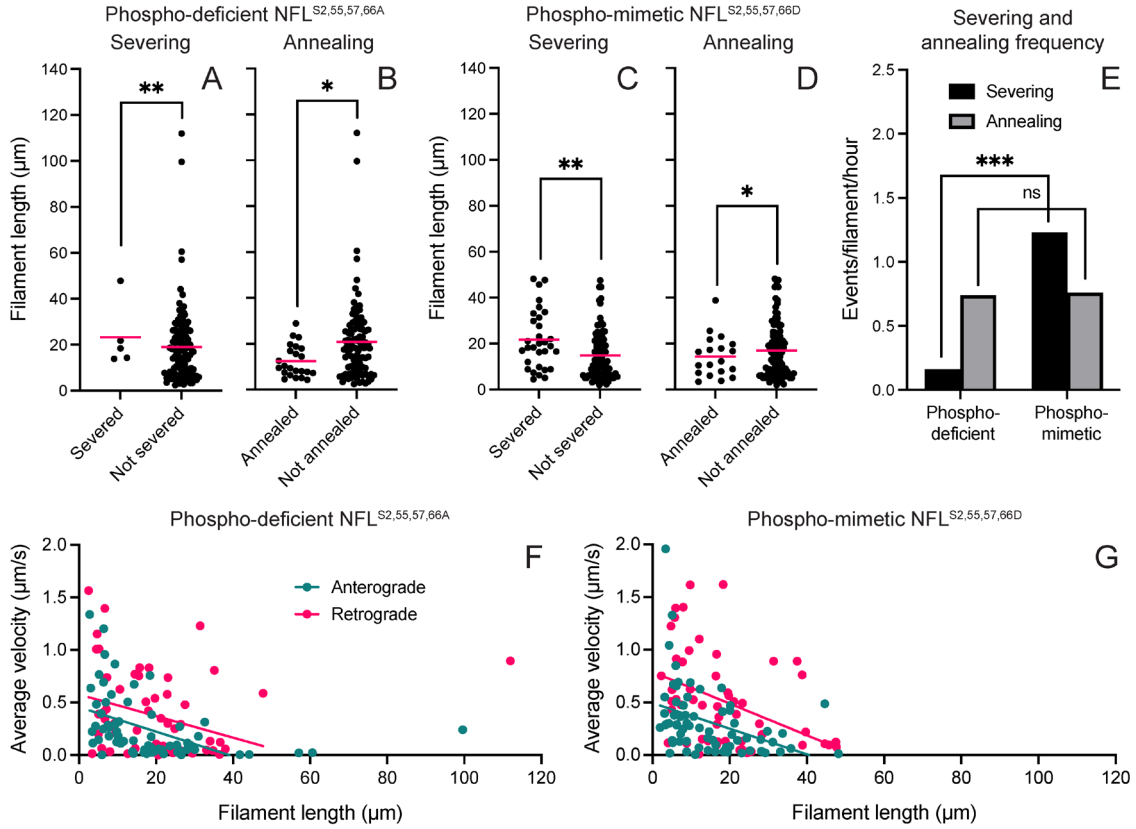

FIGURE 6: Phosphomimetic and phosphodeficient NFL mutants alter neurofilament severing frequency. Data from multifield time-lapse movies of neonatal rat cortical neurons expressing either NFL^{S2,55,57,66A}-GFP (phosphodeficient mutant) or NFL^{S2,55,57,66D}-GFP (phosphomimetic mutant) after 8–10 d in culture. (A–D) Dot plots of filament length for filaments that either annealed or did not anneal and that either severed or did not sever during the period of observation. Data from 122 filaments in 73 movies for phosphodeficient NFL (total observation time = 31.2 h; average movie duration = 25.6 min) and 122 filaments in 68 movies for phosphomimetic NFL (total observation time = 25.2 h; average movie duration = 22.5 min). Note that there was no significant difference between the length dependence of severing and annealing in the presence of phosphomimetic and phosphodeficient NFL. For both mutants, long filaments severed more frequently than short filaments ($p = 0.0063$ in A and C) and short filaments annealed more frequently than long filaments ($p = 0.012$ in B and D). The horizontal magenta lines represent the population means. Note that in the presence of phosphodeficient NFL, we encountered four filaments that were longer than 50 μm (specifically 57, 61, 100, and 112 μm). (E) The average severing and annealing frequencies for the data in A–D. Note that severing is enhanced in filaments containing phosphomimetic NFL compared with phosphodeficient NFL ($p < 0.0001$), whereas annealing frequency is unaffected ($p = 0.407$). (F, G) Average velocity plotted vs. filament length for filaments that moved in a net anterograde (teal) or retrograde (magenta) direction. There was a statistically significant effect of direction ($\beta = -0.19$, SE = 0.04, $p < 0.0001$) and length ($\beta = -0.012$, SE = 0.0019, $p < 0.0001$) on velocity but no significant effect difference between the mutants ($\beta = -0.73$, SE = 0.04, $p = 0.098$). The statistical analysis in A–D was performed using a logistic regression model. The statistical analysis in F and G was performed using a linear regression model, excluding two outlier filaments that measured 100 and 112 μm in the phosphodeficient data (more than five times the interquartile range above the median) to ensure that we compared filaments of similar lengths. ns ($p > 0.05$), * ($p \leq 0.05$), ** ($p \leq 0.01$), **** ($p \leq 0.001$).

treatment of cortical neurons expressing NFL^{S2,55,57,66A}-GFP, which is not phosphorylatable at these four sites, resulted in only a slight reduction in neurofilament length from 11.8 ± 8.6 μm to 11.0 ± 7.3 μm, which was not significant ($p = 0.49$) (Figure 7D; Supplemental Movie S10).

To confirm that the protective effect of the phosphodeficient NFL^{S2,55,57,66A} mutant on neurofilament length was also observed for neurofilament transport, we measured the frequency of neurofilament movement in the same fixed-field time-lapse movies. In NFL$^{-/-}$ knockout neurons expressing wild-type NFL-GFP, treatment with 8-Br-cAMP plus OA increased the average frequency of neurofilament movement from 6.5 ± 7.0 filaments/axon/h to 19.3 ± 13.5 filaments/axon/h ($p < 0.0001$) (Figure 7E). In neurons expressing NFL^{S2,55,57,66A}-GFP, there was as significant reduction in transport frequency to 3.7 ± 4.5 filaments/axon/h ($p < 0.0001$), which reflects the increase in filament length, but no change in transport frequency upon treatment with 8-Br-cAMP plus OA ($p = 0.85$) (Figure 7F). Thus, phosphodeficient NFL^{S2,55,57,66A}-GFP increased filament length, decreased filament transport frequency, and protected the neurofilaments from the effects of PKA activation. These data indicate that the effect of PKA activators on neurofilament length and transport was dependent on phosphorylation of NFL and that the kinase acts on one or more of the four sites mutated in the NFL^{S2,55,57,66A}-GFP construct.

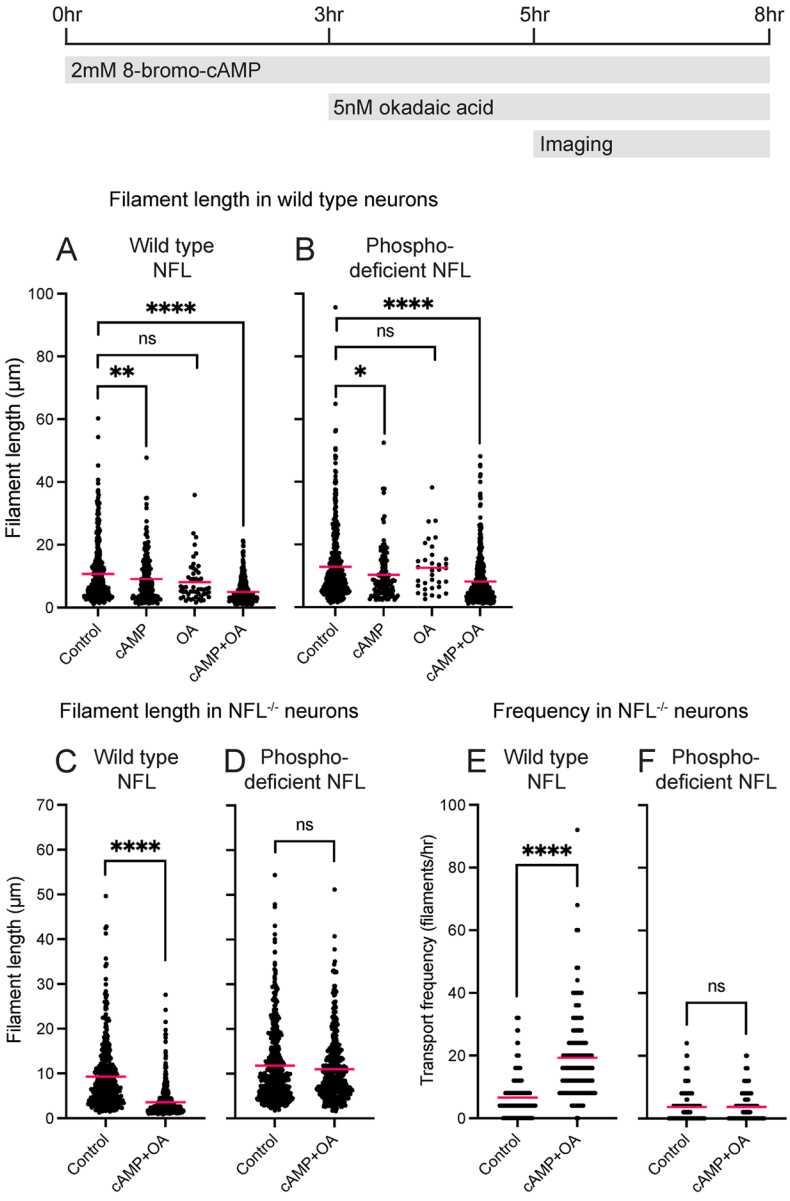

FIGURE 7: Phosphodeficient mutant NFL protects neurofilaments against the effect of PKA activators. (A, B) Dot plots of neurofilament length in neonatal rat cortical neurons after 12–14 d in culture (148 movies, average duration = 15 min, total of 2212 neurofilaments). The neurons were transfected with wild-type rat NFL-GFP (A) or phosphodeficient mutant rat NFL^{S2,55,57,66A}-GFP (B) and treated with vehicle, 8-bromo-cAMP (cAMP), OA, or 8-bromo-cAMP plus OA. Note that treatment with cAMP but not OA reduced neurofilament length in neurons expressing wild-type NFL and the effect was more marked for neurons treated with cAMP and OA together. The same treatments also reduced neurofilament length in neurons expressing phosphodeficient NFL, but the extent of the reduction was smaller. There was a significant difference between the cAMP plus OA treatment compared with treatment with either cAMP alone or OA alone, and this was so for both the wild-type and phosphodeficient NFL ($p < 0.0001$ in all cases). However, there was no significant difference between the cAMP and OA treatments for either the wild-type ($p = 0.75$) or phosphodeficient ($p = 0.10$) NFL. (C, D) Dot plots of neurofilament length in neonatal mouse cortical neurons from NFL knockout mice after 8–10 d in culture (77 movies, average duration = 15 min, total of 1768 neurofilaments tracked). The neurons were transfected with wild-type NFL-GFP (C) or phosphodeficient mutant NFL^{S2,55,57,66A}-GFP (D) and then treated with vehicle or 8-bromo-cAMP and OA. The schematic above the plots shows the experimental timeline, which involved pretreatment for 3 h with 8-bromo-cAMP, treatment for 2 h in the presence of 8-bromo-cAMP plus OA, and imaging for up to 3 h in the continued presence of these reagents. Note that the treatment reduced neurofilament length in neurons expressing wild-type NFL but not in neurons expressing phosphodeficient NFL. (E, F) Dot plots of neurofilament transport frequencies at 8–11 d. We measured 3764 filaments in 290 axons in 41 movies for the wild-type NFL and 1380 filaments in 376 axons in 50 movies for phosphodeficient NFL. The statistical analysis was performed using a linear regression model in A–D and a Poisson regression model in E and F. The horizontal magenta lines represent the population means. ns ($p > 0.05$), * ($p \leq 0.05$), ** ($p \leq 0.01$), **** ($p \leq 0.0001$).

DISCUSSION

We have used live-cell imaging to investigate the dynamics of neurofilament severing and end-to-end annealing in cultured neurons. Our data establish that severing and annealing are robust and quantifiable features of neurofilament dynamics in neurons that regulate neurofilament length, which in turn has a profound influence on the long-term transport behavior of these cytoskeletal polymers. Severing creates shorter filaments, which move more persistently, pausing and reversing less often. On the other hand, annealing creates longer filaments, which pause and reverse direction more often, resulting in less net movement. Our data also reveal a novel dependency of filament severing and annealing on neurofilament length. Long filaments sever more frequently and anneal less frequently, whereas short filaments sever less frequently and anneal more frequently. Thus, neurofilaments undergo a dynamic cycle of severing and end-to-end annealing in axons that regulates neurofilament length and transport (Figure 8A).

According to this model, neurofilament length is determined by the balance of the annealing and severing rates. At steady state, which may be achieved in mature nongrowing axons, the two rates would be balanced. In our cultures, where the average neurofilament length increased with time, we thus expected to observe more annealing than severing in our time-lapse movies. However, we observed about twice as many severing events as annealing events. A possible explanation for this is that we can detect annealing and severing only in axonal regions that have very low neurofilament content, where single filaments can be observed in isolation, yet annealing requires an encounter between two filament ends and thus may be less likely when neurofilament density is low. In contrast, severing does not require a diffusional encounter between filaments and thus may be independent of filament density. Thus, our observations in these cultured neurons may underestimate the rate of annealing that would be encountered in more neurofilament-rich axons.

The mechanism of the length dependence of neurofilament movement, severing, and annealing is an interesting question. The length dependence of the pauses and reversals could be explained if the number of motors recruited by the filaments is proportional

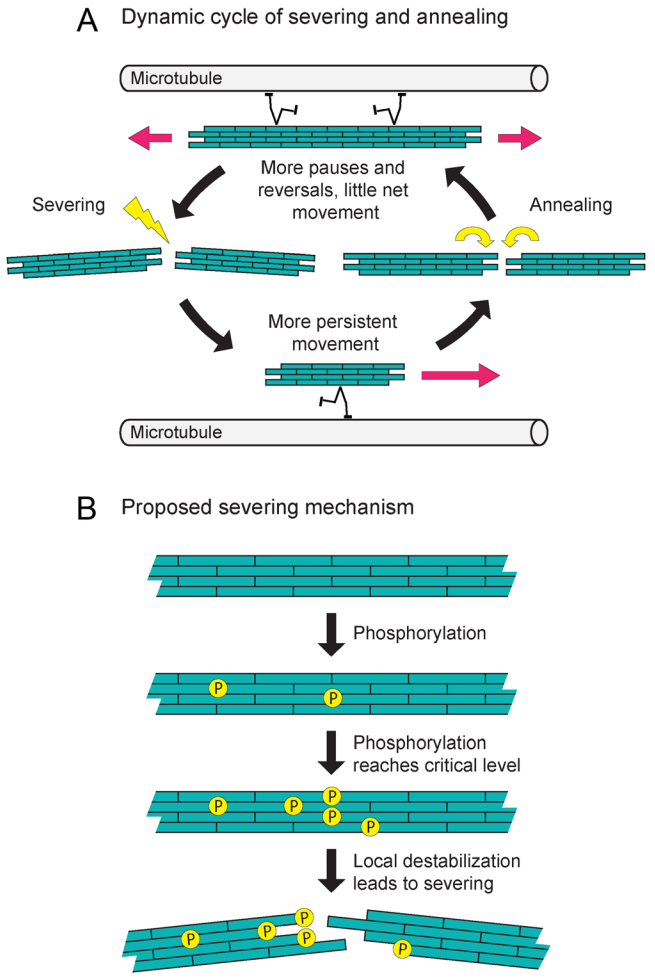

FIGURE 8: Regulation of neurofilament transport by a dynamic cycle of neurofilament severing and annealing. (A) Schematic diagram of the cycle of neurofilament severing and annealing described in this study. Neurofilaments move along microtubule tracks (magenta arrows). Severing generates shorter filaments that move more persistently in either the anterograde or the retrograde direction, pausing and reversing less often. Annealing generates longer filaments, which pause and reverse direction more often, resulting in little net movement. Short filaments anneal more frequently than long filaments, whereas long filaments sever more frequently than short filaments. The result is a dynamic cycle of severing and annealing that regulates neurofilament transport. Note that it is likely that there are multiple mechanisms of neurofilament transport regulation. For example, there is evidence that neurofilament pausing can also be regulated by phosphorylation of the C-terminal tail domain of NFH (Ackerley *et al.*, 2003). However, for clarity, we depict only severing and annealing in this figure. (B) Proposed severing mechanism. Phosphorylation of subunits in the neurofilament polymer weakens their affinity for each other. When the number of phosphorylated subunits reaches a certain critical load, it can destabilize the polymer at that location and cause the polymer to break.

to the filament length. Short filaments might recruit on average one motor, leading to persistent unidirectional movement, whereas long filaments might recruit on average multiple motors that could be of opposite directionality. The latter would result in a sort of dynamic tug-of-war that might cause long filaments to stall for prolonged periods or shuttle between alternating anterograde and retrograde bouts, resulting in little net movement (Dallon *et al.*, 2019; Portet *et al.*, 2019). With respect to the length dependence of neurofilament severing and annealing, it is possible that long filaments anneal less frequently simply because they are less mobile and thus collide less frequently and that they sever more frequently simply because longer polymers have more potential severing sites. However, it is also possible that these differences between long and short filaments reflect differences in their composition, posttranslational modification, or interactions with other cytoplasmic components.

To investigate the effect of phosphorylation on neurofilament length and transport, we used site-directed mutagenesis. Expression of phosphomimetic NFL ($NFL^{S2,55,57,66D}$) resulted in shorter neurofilaments that moved and severed more frequently, whereas phosphodeficient NFL ($NFL^{S2,55,57,66A}$) had the opposite effect. Remarkably, filaments containing phosphodeficient NFL reached lengths of up to 112 µm, which is the longest moving filament that we have ever encountered. Treatment with activators of PKA reduced neurofilament length, and this effect was blocked by mutating serines 2, 55, 62, and 66 in the NFL head domain to alanines. These observations suggest that N-terminal phosphorylation of NFL could be a mechanism for neurofilament severing. Consistent with this severing model, neurofilaments containing phosphodeficient NFL exhibited lower rates of severing, while filaments containing phosphomimetic NFL exhibited higher rates of severing.

Because neurofilaments contain ~32 polypeptides per cross-section (Heins *et al.*, 1993), severing likely requires the phosphorylation of multiple subunit proteins at the same location along the polymer, with each additional phosphorylated subunit further weakening the filament at that location and increasing the severing probability (Figure 8B). While the phosphorylation could be random, it is more likely to occur locally downstream of local signaling events that may be spatially or temporally controlled to regulate neurofilament length and transport. Severing cannot be generated simply by the pulling force of molecular motors because it takes nanonewtons of force to stretch and break single intermediate filaments (Kreplak *et al.*, 2005, 2008; Guzman *et al.*, 2006), but it is possible that such a pulling force could break a filament that is weakened by local phosphorylation events. In this regard, it is interesting to note that the severing events in our movies often appear to occur when the filaments begin to move. However, because severing cannot be confirmed until the daughter fragments move apart, we cannot rule out the possibility that these filaments were severed spontaneously before the onset of movement.

We focused on PKA in this study because it has been reported to phosphorylate three of the sites mutated in our phosphomimetic and phosphodeficient NFL constructs. However, we do not exclude the possible involvement of other kinases, phosphorylation sites, and/or neurofilament subunits. PKA can phosphorylate the head domains of peripherin, NFM, and neurofilament protein H (NFH) in addition to NFL (Huc *et al.*, 1989; Hisanaga *et al.*, 1994; Cleverley *et al.*, 1998; Giasson and Mushynski, 1998; Sihag *et al.*, 1999), and the NFL head domains can be phosphorylated by protein kinase C (PKC), rho kinase, protein kinase N (PKN), and CaMKII (Gonda *et al.*, 1990; Sihag and Nixon, 1991; Sihag *et al.*, 2007; Hisanaga *et al.*, 1994; Mukai *et al.*, 1996; Hashimoto *et al.*, 1998, 2000; Nakamura *et al.*, 2000). PKC has also been reported to phosphorylate NFM and NFH (Sihag *et al.*, 1988) and has been shown to induce intermediate filament disassembly in vitro and in cultured cells (Hisanaga *et al.*, 1990, 1994; Giasson *et al.*, 1996). Nonetheless, our data indicate that treatment with cyclic adenosine monophosphate (cAMP) and OA is sufficient to induce neurofilament severing. We recognize that the phosphatases inhibited by OA are not specific for PKA pathways and that PKA phosphorylation has other roles in axons.

However, the fact that phosphodeficient NFL rescued the effect of cAMP and OA on filament length in NFL knockout neurons confirms that phosphorylation at one or more of the mutated sites is required for the experimentally induced neurofilament severing. Because head domain phosphorylation by PKA also induces disassembly of vimentin and keratin filaments (Inagaki *et al.*, 1987; Evans, 1988; Ando *et al.*, 1989, 1996; Eriksson *et al.*, 2004), focal destabilization of intermediate filaments by N-terminal phosphorylation of their constituent polypeptides at specific locations along their length may be a general mechanism for severing this class of cytoskeletal polymers. In this way, phosphorylation at discrete sites along intermediate filaments may represent another tool in the toolbox that cells can use to regulate the organization and dynamics of this class of cytoskeletal polymers.

The axonal transport of neurofilaments is known to slow both spatially and temporally during postnatal development of myelinated axons (Hoffman *et al.*, 1983, 1985; Xu and Tung, 2001; Jung and Brown, 2009). This contributes to the accumulation of neurofilaments that drives the expansion of myelinated axon caliber (Cleveland *et al.*, 1991; Hoffman, 1995). The mechanism of this slowing has been attributed to an increase in phosphorylation of the carboxy-terminal tail domains of neurofilament proteins M and H (Sanchez *et al.*, 2000; Ackerley *et al.*, 2003; Garcia *et al.*, 2003; Rao *et al.*, 2003). However, deleting these domains or mutating them to block phosphorylation did not impair neurofilament transport or accumulation in vivo (Rao *et al.*, 2002; Yuan *et al.*, 2006; Garcia *et al.*, 2009). Thus, the role of neurofilament tail domain phosphorylation in the regulation of neurofilament transport is currently unclear. We have proposed previously that neurofilament transport could also be slowed by shifting the balance of anterograde and retrograde movement so as to increase the proportion of the time that the filaments move backward (Jung and Brown, 2009). On the basis of the data presented above, we speculate that an additional mechanism for slowing neurofilament transport may be the modulation of neurofilament length by spatial and temporal regulation of the cycle of neurofilament severing and annealing (e.g., by modulation of the activities of PKA and PP2A). For example, a shift in these activities to favor annealing over severing during axonal maturation would result in an increase in average neurofilament length and a decrease in net transport velocity. In a recent computational study, we have shown that for a given flux, a decrease in neurofilament transport velocity in a given segment of axon results in an increase in the residence time of the neurofilaments, leading to an increase in the neurofilament content (Nowier *et al.*, 2023). In this way, neurofilament severing and annealing may represent a mechanism to regulate the neurofilament content and diameter of axons, which is an important influence on their conduction velocity.

MATERIALS AND METHODS

Molecular cloning

The rat pNFL-myc, pNFL^{S2,55,57,66A}-myc, pNFL^{S2,55,57,66D}-myc, pNFL^{S2A}, pNFL^{S2D}, pNFL^{S55A}, pNFL^{S55D}, pNFL^{S57A}, pNFL^{S57D}, pNFL^{S66A}, and pNFL^{S66D} cDNA expression constructs were provided by Chris Miller (King's College, University of London; Yates *et al.*, 2009). The pNFL-myc, pNFL^{S2,51,55,66A}-myc, and pNFL^{S2,55,57,66D}-myc constructs encoded a myc epitope tag linked to the C-terminus of rat NFL. To make the pNFL-GFP, pNFL^{S2,55,57,66A}-GFP, and pNFL^{S2,55,57,66D}-GFP fluorescent fusion constructs, we used PCR to amplify the NFL sequences in the pNFL-myc, pNFL^{S2,51,55,66A}-myc, and pNFL^{S2,55,57,66D}-myc constructs and then cloned these sequences into the pEGFP-N3 vector (Clontech/Takara Bio) between the *Eco*R1 and *Bam*H1 restriction sites of the multiple cloning site. The forward and reverse PCR primers were 5′-CGA CTC ACT ATA GGC TAG CCT CGA GAA TTC CTG AGG-3′ and 5′-CGC GGA TCC ATC TTT CTT AGC TTG C-3′, respectively. The resulting vectors coded for GFP linked to the C-terminus of rat NFL by a five-amino-acid linker with the sequence -Gly-Ser-Ile-Ala-Thr-. To make the mouse pNFL-GFP fluorescent fusion construct, we first amplified the mouse NFL coding region by PCR using the mouse pNFL-paGFP construct (Uchida *et al.*, 2013) as a template. The forward and reverse PCR primers were 5′-CAT TGA CGC AAA TGG GCG GTA G-3′ and 5′-CGG GAT CCA TCT TTC TTA GCC AC-3′, respectively. This PCR product was then cloned into the rat pNFL-GFP construct between the *Nhe*I and *Bam*H1 sites to replace the rat sequence with the mouse sequence. To make the mouse pNFL^{S2,55,57,66A}-GFP and pNFL^{S2,55,57,66D}-GFP fluorescent fusion constructs, we used custom gene synthesis (GenScript, USA) to create 361-base-pair DNA fragments spanning the first 99 codons of the mouse NFL cDNA (with either the S2,55,57,66A or S2,55,57,66D mutations) flanked by *Xho*I and *Pvu*I restriction sites. We then cloned these fragments between the *Xho*I and *Pvu*I restriction sites in the mouse pNFL-GFP construct. The resulting vectors coded for GFP linked to the C-terminus of mouse NFL by a five-amino-acid linker with the sequence -Gly-Ser-Ile-Ala-Thr-, identical to the linker in the rat constructs. All constructs were confirmed by sequencing the entire open reading frame.

A note about the residue numbering in NFL

There is some inconsistency between the literature and genomic sequence databases concerning the numbering of the amino acid residues in the NFL head domain. NFL was first sequenced by Edman degradation and found to lack the N-terminal methionine and thus start with a serine (Geisler *et al.*, 1985). This was subsequently confirmed by others using mass spectrometry, and the N-terminal serine was found to be acetylated (Betts *et al.*, 1997; Cleverley *et al.*, 1998; Trimpin *et al.*, 2004), which suggests that the N-terminal methionine is removed posttranslationally. Thus, the early literature on NFL phosphorylation numbered the phosphorylation sites in the protein starting from the second amino acid residue in the NFL open reading frame, and this has continued to the present day (e.g., Giasson *et al.*, 1996; Hashimoto *et al.*, 2000; Nakamura *et al.*, 2000; Yates *et al.*, 2009). To avoid confusion and maintain consistency with the published literature, we chose to retain this numbering. Thus, the serines mutated in the present study are referred to as serines 2, 55, 57, and 66 even though they are actually in positions 3, 56, 58, and 67 of the predicted translation product.

NFL knockout mice

NFL$^{+/-}$ heterozygous mice (Zhu *et al.*, 1997) were obtained from Don Cleveland at the University of California, San Diego, and maintained heterozygous in our facility by crossing with wild-type C57BL/6 mice. NFL$^{-/-}$ homozygotes were obtained in the expected Mendelian proportions by crossing heterozygotes. Genotyping was performed by PCR using tail DNA with forward primer 5′-GCT ATT CGG CTA TGA CTG GGC ACA A-3′ and reverse primer 5′-CGA TGT TTC GCT TGG TCG AAT G -3′, which resulted in amplification of the neo cassette inserted in exon 1. The wild-type allele was detected using forward primer 5′-GCA ACG ACC TCA AGT CTA TCC GCA-3′ and reverse primer 5′-CTT CGG CGT TCT GCA TGT TCT TGG -3′. The sizes of the amplified PCR products were 366 and 597 base pairs, respectively.

Cell culture and transfection

Cortical neurons from mice and rats were cultured using the glial sandwich technique of Kaech and Banker (2006) as modified by

Uchida *et al.* (2016). We used rat glia for both rat and mouse neuronal cultures. To prepare glial cultures, the cerebral cortices of 4 to 6 postnatal day 0 (P0) rats were dissociated and chopped in Ca^{++}/Mg^{++}-free Hank's balanced salt solution (HBSS; Invitrogen, Carlsbad, CA). The tissue pieces were dissociated in phosphate-buffered saline (PBS) containing 0.25% (wt/vol) trypsin (Worthington Biochemical Corp., Lakewood, NJ), 0.1% (wt/vol) DNase-I (Sigma, St. Louis, MO), and 0.27 mM EDTA (Sigma). The resulting cell suspension was plated in a 75 cm^3 flask and maintained at 37°C in glial medium consisting of MEM (Invitrogen) supplemented with 10% (vol/vol) horse serum (Invitrogen), 0.7% (wt/vol) glucose (Sigma), and 5 μg/ml gentamicin (Invitrogen), in an atmosphere of 5% CO_2. After 2 h, the flask was swirled to remove loosely attached cells and then fed with fresh glial medium. The cells were typically passaged just once about 2 d before the intended day of use and plated on glass-bottomed dishes coated with poly-D-lysine (Sigma). The glial medium was replaced with neuronal plating medium (see below) on the day of use.

To prepare neuronal cultures, the cerebral cortex of one P0 rat or mouse was dissociated in HBSS and dissociated in PBS containing 0.25% (wt/vol) trypsin, 0.27 mM EDTA (Sigma), and 0.1% (wt/vol) DNase-I for each transfection. The resulting cortical neurons were transfected before plating by electroporation using an Amaxa Nucleofector (Lonza, Walkersville, MD) with the rat neuron Nucleofection kit (VPG-1003) and program G013 or mouse neuron kit (VPG-1001) and program O005. The volume of the cell suspension was 100 μl, and the cell density ranged from 4 to 6×10^6 cells/ml. The DNA consisted of a mixture of 5 μg of the pNFL-GFP construct, 5 μg of the pNFM construct, and 5 μg of the EB3-mCherry construct. We used rat constructs when transfecting rat neurons and mouse constructs when transfecting mouse neurons. The cells were then plated onto glass-bottomed dishes coated with poly-D-lysine. Glass coverslips bearing glia (>80% confluency) were suspended cell-side down over the neurons using dots of paraffin wax as spacers. The resulting sandwich cultures were maintained initially at 37°C/5%CO_2 in neuronal plating medium, which consisted of NbActiv4 (BrainBits; Brewer *et al.*, 2008) supplemented with 5% (vol/vol) fetal bovine serum (FBS; Thermo Scientific) and 5 μg/ml gentamicin. On the day after plating, this medium was replaced with neuronal culturing medium. The neuronal culturing medium was identical to the plating medium except that it lacked serum and contained 5 μM cytosine arabinoside (AraC; Sigma). Every 2 d, half the medium was removed and replaced with fresh medium.

Human adrenal adenocarcinoma SW13vim- cells, which lack endogenous vimentin (Sarria *et al.*, 1990), were cultured in DMEM/F12 (Thermo Fisher Scientific) supplemented with 5% FBS (HyClone; GE Healthcare, Chicago, IL) and 10 μg/ml gentamicin (MilliporeSigma, Burlington, MA). The cells were transfected with Lipofectamine 2000 (Thermo Fisher Scientific) as described previously (Colakoglu and Brown, 2009; Stone *et al.*, 2019).

Protein kinase A activation

8-bromo cAMP and/or OA were added directly to the culture medium at final concentrations of 2 mM and 5 nM, respectively. The incubation time before imaging was 5 h for 8-bromo-cAMP and 2 h OA. For combined treatment with both reagents, we first added 8-bromo cAMP, incubated for 3 h, and then added OA. After incubation for an additional 2 h, the cells were kept in the medium containing the two reagents and imaged for up to 5 h.

Microscopy and imaging

For imaging, the neuronal cell culture medium was replaced with Hibernate-A medium (BrainBits; low-fluorescence formulation) supplemented with 2% (vol/vol) B27 supplement mixture, 0.5 mM Glutamax (Invitrogen), and 37.5 mM NaCl to increase the osmolarity to ~310–320 mOs. To maintain the temperature at 37°C, we used a stage-top incubator with a humidity module (Okolab, Ottaviano, Naples, Italy) and an objective heater (Bioptechs, Butler, PA). The cells were observed with a Nikon TiE inverted wide-field epifluorescence microscope equipped with a 100×/1.4NA Plan-Apochromat VC oil immersion objective, SOLA LED light source (Lumencor, Beaverton, OR), and Nikon TI-S-ER motorized stage with X-Y linear encoders. The exciting light was attenuated to 10–15% transmission using the LED light source controller. Images were acquired with no pixel binning using an Andor iXon Ultra 897 EMCCD camera (Andor Technology, Belfast, UK), which has a 512×512 array of 16×16 μm pixels, and MetaMorph software (Molecular Devices, Sunnyvale, CA). The GFP and mCherry fluorescence was imaged using an ET-GFP filter cube (model 49002; Chroma Technology, Brattleboro, VT) or an ET-mCherry/Texas Red filter cube (model 49008; Chroma). The movement of GFP-tagged neurofilaments was recorded by acquiring time-lapse movies for a duration of 15 or 30 min using 100 ms exposures and 3 s time intervals. For our analyses of the frequency of neurofilament movement, the movies were acquired at a fixed location, which we refer to as fixed-field time-lapse movies. For our analyses of the long-term kinetic behavior of single neurofilaments, we acquired multifield time-lapse movies by moving the field of view during the acquisition (described below). The movement of EB3-mCherry comets was recorded by acquiring fixed-field time-lapse movies for a duration of 5 min using 1 s exposures and 3–5 s time intervals. To compare axon width and neurofilament content in the cortical neuron cultures, overlapping images were acquired along the entire length of multiple axons. Montages were created in the FIJI distribution package of ImageJ (Schindelin *et al.*, 2012) using the Pairwise Stitching plug-in (Preibisch *et al.*, 2009). The images were all acquired with the same exposure and subjected to the same intensity scaling. The axon width was taken to be the width at half height on a linear intensity profile (line width = 11 pixels) drawn perpendicular to the long axis of the axon, measured at the midpoint of the axon within each image of the montage, that is, at ~200–300 μm intervals along the axons.

Multifield tracking

This method takes advantage of the motorized stage on our microscope and the "Move stage to image position" function in the MetaMorph software to recenter the filament whenever it approaches the edge of the camera field of view (Uchida *et al.*, 2016). First, we selected an isolated filament to track by observing the acquired images live during time-lapse image acquisition. In selecting filaments to track, we sought to track similar numbers in the range 0–10, 10–20, and >20 μm to ensure even sampling across a broad range of filament lengths. When the selected filament approached the edge of the camera field of view, we clicked on it. This caused the stage to move automatically to center the filament within the field of view. By repeating this process, it was possible to track single filaments along axons over distances of 1 mm or more. Our time-lapse interval of 3 s was sufficient time to allow the mouse to be clicked, the stage to move, and the new stage position to register before the next image is acquired, thereby allowing continuous time-lapse acquisition of the moving filament. We aimed to follow each filament for 30 min, but we terminated the acquisition earlier than that if the filament reached the end of the axon, entered either the cell body or the growth cone, or was lost due to overlap with other filaments. To confirm axon orientation, we acquired a fixed-field time-lapse movie of the EB3-mCherry fluorescence and tracked

the direction of movement of EB3 comets, which corresponds to the anterograde direction (Fenn *et al.*, 2018a). Axons with ambiguous directionality were excluded from our analysis.

To track neurofilament movement in the multifield time-lapse movies, the image planes were stitched together using the *x*–*y* coordinates of the stage positions to create a multifield montage from the movie planes (Uchida *et al.*, 2016). The *x*–*y* coordinates of one end of the filament were then recorded in successive movie frames using the "TrackPoints" option in the Motion analysis drop-in of the MetaMorph software. To be consistent, for each filament we selected the end that was leading when the filament was moving in its net direction of movement and tracked that same end throughout the movie. The coordinates and other parameters such as elapsed time, direction, and velocity were logged to a Microsoft Excel spreadsheet via Dynamic Data Exchange for further analysis.

Analysis of neurofilament movement, severing, and annealing

For the multifield time-lapse movies, we tracked filaments greater than or equal to 10 pixels (1.6 µm) in length that moved a total distance of at least 50 pixels (8 µm). The net velocity was calculated by dividing the net distance moved by each filament during each movie by the elapsed time. Because neurofilaments can exhibit frequent folding behaviors while they are pausing but are almost always fully extended when they move (Fenn *et al.*, 2018b), we measured filament length only during bouts of movement. To avoid motion blurring, we made these measurements during brief pauses that interrupt these bouts of movement. To quantify annealing frequency, we counted only those events in which the adjoined filaments moved together as one after the putative annealing event. We measured the filaments before and after the putative annealing event to ensure conservation of length. To quantify severing frequency, we counted only those events in which the filament moved before breaking (to be sure that it was indeed a single filament) and in which there was clear separation between the resulting fragments (e.g., due to movement of one or both fragments). For the fixed-field time-lapse movies, which were used to quantify the frequency of neurofilament movement, we located the midpoint of the longest gap in the neurofilament array in the field of view and drew a line perpendicular to the axon at that location. We then counted the filaments that moved across each line during that movie and divided that number by the duration of the movie. If there were multiple gaps along a single axon, we selected the longest for our analysis; we did not analyze more than one gap per axon.

Immunofluorescence microscopy

Neurons were fixed with 4% formaldehyde and then extracted with PBS containing 1% (vol/vol) Triton X-100 and 0.3 M NaCl. After fixation and extraction, the cells were incubated sequentially with a mouse monoclonal specific for phosphoindependent NFM (RMO270; Invitrogen; 1:400) and a rabbit polyclonal antibody specific for the myc tag (71D10: Cell Signaling; 1:100). The secondary antibodies were Alexa 488-goat anti-mouse (Invitrogen; 1:200) and Alexa 568-goat anti-rabbit (Invitrogen; 1:200). Coverslips were mounted using ProLong Gold Antifade reagent (Invitrogen). Images were acquired on an Andor Revolution WD spinning-disk confocal, which incorporates a Yokogawa CSU-W1 confocal scanning unit, Nikon TiE inverted microscope, 100× Plan Apo 1.0 NA oil immersion objective and Andor iXon Ultra 897 EMCCD camera. SW13vim- cells were fixed with 4% formaldehyde in PBS and immunostained as described above. Images were acquired on the same microscope but using an Andor Neo sCMOS camera.

Statistical analysis

The relationships between filament length and transport frequency, velocity, or pausing in Figures 2, 6, and 7 were tested using a linear regression model. The relationships between filament length and the probability of annealing or severing in Figures 3 and 6 were tested using a logistic regression model. The effects of NFL phosphorylation or activators of PKA on filament length in Figures 5 and 7 were tested using a linear regression model. Filament lengths were natural log-transformed to better approximate normality of the residuals. The effect of NFL phosphorylation on transport frequency in Figures 5 and 7 was tested using a Poisson regression model. A two-sided significance level of $\alpha = 0.05$ was used for all tests. The analyses were performed in SAS version 9.4 (SAS, Cary, NC). Statistical significance is represented in the figures as follows: ns, $p > 0.05$, *$p \le 0.05$, **$p \le 0.01$, ***$p \le 0.001$, ****$p \le 0.0001$.

ACKNOWLEDGMENTS

We thank Chris Miller (King's College, University of London) for sharing the rat phosphomimetic and phosphodeficient NFL constructs, Robert Evans (University of Colorado, Denver) for providing the SW13vim- cell line, Don Cleveland (University of California, San Diego) for providing the NFL knockout mice originally generated by Jean-Pierre Julien (Université Laval), and Sontoria King for comments on the manuscript. This work was supported by National Institutes of Health Grants R01 NS038526, P30 NS104177, and S10 OD010383 to A. B. and by a grant from the Takeda Science Foundation to A.U.

REFERENCES

Ackerley S, Thornhill P, Grierson AJ, Brownlees J, Anderton BH, Leigh PN, Shaw CE, Miller CC (2003). Neurofilament heavy chain side arm phosphorylation regulates axonal transport of neurofilaments. J Cell Biol 161, 489–495.

Ando S, Tanabe K, Gonda Y, Sato C, Inagaki M (1989). Domain- and sequence-specific phosphorylation of vimentin induces disassembly of the filament structure. Biochemistry 28, 2974–2979.

Ando S, Tokui T, Yano T, Inagaki M (1996). Keratin 8 phosphorylation in vitro by cAMP-dependent protein kinase occurs within the amino- and carboxyl-terminal end domains. Biochem Biophys Res Commun 221, 67–71.

Betts JC, Blackstock WP, Ward MA, Anderton BH (1997). Identification of phosphorylation sites on neurofilament proteins by nanoelectrospray mass spectrometry. J Biol Chem 272, 12922–12927.

Black MM, Keyser P, Sobel E (1986). Interval between the synthesis and assembly of cytoskeletal proteins in cultured neurons. J Neurosci 6, 1004–1012.

Brewer GJ, Boehler MD, Jones TT, Wheeler BC (2008). NbActiv4 medium improvement to Neurobasal/B27 increases neuron synapse densities and network spike rates on multielectrode arrays. J Neurosci Methods 170, 181–187.

Brown A (2000). Slow axonal transport: stop and go traffic in the axon. Nat Rev Mol Cell Biol 1, 153–156.

Chou YH, Opal P, Quinlan RA, Goldman RD (1996). The relative roles of specific N- and C-terminal phosphorylation sites in the disassembly of intermediate filament in mitotic BHK-21 cells. J Cell Sci 109(Pt 4), 817–826.

Cleveland DW, Monteiro MJ, Wong PC, Gill SR, Gearhart JD, Hoffman PN (1991). Involvement of neurofilaments in the radial growth of axons. J Cell Sci 15, 85–95.

Cleverley KE, Betts JC, Blackstock WP, Gallo JM, Anderton BH (1998). Identification of novel in vitro PKA phosphorylation sites on the low and middle molecular mass neurofilament subunits by mass spectrometry. Biochemistry 37, 3917–3930.

Colakoglu G, Brown A (2009). Intermediate filaments exchange subunits along their length and elongate by end-to-end annealing. J Cell Biol 185, 769–777.

Dallon JC, Leduc C, Etienne-Manneville S, Portet S (2019). Stochastic modeling reveals how motor protein and filament properties affect intermediate filament transport. J Theor Biol 464, 132–148.

Eriksson JE, He T, Trejo-Skalli AV, Harmala-Brasken AS, Hellman J, Chou YH, Goldman RD (2004). Specific in vivo phosphorylation sites determine the assembly dynamics of vimentin intermediate filaments. J Cell Sci 117, 919–932.

Evans RM (1988). Cyclic AMP-dependent protein kinase-induced vimentin filament disassembly involves modification of the N-terminal domain of intermediate filament subunits. FEBS Lett 234, 73–78.

Fenn JD, Johnson CM, Peng J, Jung P, Brown A (2018a). Kymograph analysis with high temporal resolution reveals new features of neurofilament transport kinetics. Cytoskeleton (Hoboken) 75, 22–41.

Fenn JD, Monsma PC, Brown A (2018b). Axonal neurofilaments exhibit frequent and complex folding behaviors. Cytoskeleton (Hoboken) 75, 258–280.

Francis F, Roy S, Brady ST, Black MM (2005). Transport of neurofilaments in growing axons requires microtubules but not actin filaments. J Neurosci Res 79, 442–450.

Garcia ML, Lobsiger CS, Shah SB, Deerinck TJ, Crum J, Young D, Ward CM, Crawford TO, Gotow T, Uchiyama Y, *et al*. (2003). NF-M is an essential target for the myelin-directed "outside-in" signaling cascade that mediates radial axonal growth. J Cell Biol 163, 1011–1020.

Garcia ML, Rao MV, Fujimoto J, Garcia VB, Shah SB, Crum J, Gotow T, Uchiyama Y, Ellisman M, Calcutt NA, Cleveland DW (2009). Phosphorylation of highly conserved neurofilament medium KSP repeats is not required for myelin-dependent radial axonal growth. J Neurosci 29, 1277–1284.

Geisler N, Plessmann U, Weber K (1985). The complete amino acid sequence of the major mammalian neurofilament protein (NF-L). FEBS Lett 182, 475–478.

Giasson BI, Cromlish JA, Athlan ES, Mushynski WE (1996). Activation of cyclic AMP-dependent protein kinase in okadaic acid-treated neurons potentiates neurofilament fragmentation and stimulates phosphorylation of Ser^{2} in the low-molecular-mass neurofilament subunit. J Neurochem 66, 1207–1213.

Giasson BI, Mushynski WE (1998). Intermediate filament disassembly in cultured dorsal root ganglion neurons is associated with amino-terminal head domain phosphorylation of specific subunits. J Neurochem 70, 1869–1875.

Gill SR, Wong PC, Monteiro MJ, Cleveland DW (1990). Assembly properties of dominant and recessive mutations in the small mouse neurofilament (NF-L) subunit. J Cell Biol 111, 2005–2019.

Gonda Y, Nishizawa K, Ando S, Kitamura S, Minoura Y, Nishi Y, Inagaki M (1990). Involvement of protein kinase C in the regulation of assembly-disassembly of neurofilaments in vitro. Biochem Biophys Res Commun 167, 1316–1325.

Guzman C, Jeney S, Kreplak L, Kasas S, Kulik AJ, Aebi U, Forro L (2006). Exploring the mechanical properties of single vimentin intermediate filaments by atomic force microscopy. J Mol Biol 360, 623–630.

Hashimoto R, Nakamura Y, Goto H, Wada Y, Sakoda S, Kaibuchi K, Inagaki M, Takeda M (1998). Domain- and site-specific phosphorylation of bovine NF-L by Rho-associated kinase. Biochem Biophys Res Commun 245, 407–411.

Hashimoto R, Nakamura Y, Komai S, Kashiwagi Y, Tamura K, Goto T, Aimoto S, Kaibuchi K, Shiosaka S, Takeda M (2000). Site-specific phosphorylation of neurofilament-L is mediated by calcium/calmodulin-dependent protein kinase II in the apical dendrites during long-term potentiation. J Neurochem 75, 373–382.

He Y, Francis F, Myers KA, Yu W, Black MM, Baas PW (2005). Role of cytoplasmic dynein in the axonal transport of microtubules and neurofilaments. J Cell Biol 168, 697–703.

Heins S, Wong PC, Muller S, Goldie K, Cleveland DW, Aebi U (1993). The rod domain of NF-L determines neurofilament architecture, whereas the end domains specify filament assembly and network formation. J Cell Biol 123, 1517–1533.

Herrmann H, Haner M, Brettel M, Ku NO, Aebi U (1999). Characterization of distinct early assembly units of different intermediate filament proteins. J Mol Biol 286, 1403–1420.

Hisanaga S, Gonda Y, Inagaki M, Ikai A, Hirokawa N (1990). Effects of phosphorylation of the neurofilament L protein on filamentous structures. Cell Regul 1, 237–248.

Hisanaga S, Matsuoka Y, Nishizawa K, Saito T, Inagaki M, Hirokawa N (1994). Phosphorylation of native and reassembled neurofilaments composed of NF-L, NF-M, and NF-H by the catalytic subunit of cAMP-dependent protein kinase. Mol Biol Cell 5, 161–172.

Hoffman PN (1995). The synthesis, axonal transport, and phosphorylation of neurofilaments determine axonal caliber in myelinated nerve fibers. Neuroscientist 1, 76–83.

Hoffman PN, Griffin JW, Gold BG, Price DL (1985). Slowing of neurofilament transport and the radial growth of developing nerve fibers. J Neurosci 5, 2920–2929.

Hoffman PN, Lasek RJ, Griffin JW, Price DL (1983). Slowing of the axonal transport of neurofilament proteins during development. J Neurosci 3, 1694–1700.

Hookway C, Ding L, Davidson MW, Rappoport JZ, Danuser G, Gelfand VI (2015). Microtubule-dependent transport and dynamics of vimentin intermediate filaments. Mol Biol Cell 26, 1675–1686.

Huc C, Escurat M, Djabali K, Derer M, Landon F, Gros F, Portier MM (1989). Phosphorylation of peripherin, an intermediate filament protein, in mouse neuroblastoma NIE 115 cell line and in sympathetic neurons. Biochem Biophys Res Commun 160, 772–779.

Inagaki M, Nishi Y, Nishizawa K, Matsuyama M, Sato C (1987). Site-specific phosphorylation induces disassembly of vimentin filaments in vitro. Nature 328, 649–652.

Izawa I, Inagaki M (2006). Regulatory mechanisms and functions of intermediate filaments: a study using site- and phosphorylation state-specific antibodies. Cancer Sci 97, 167–174.

Jung P, Brown A (2009). Modeling the slowing of neurofilament transport along the mouse sciatic nerve. Phys Biol 6, 046002.

Kaech S, Banker G (2006). Culturing hippocampal neurons. Nat Protoc 1, 2406–2415.

Klymkowsky MW, Maynell LA, Nislow C (1991). Cytokeratin phosphorylation, cytokeratin filament severing and the solubilization of the maternal mRNA Vg1. J Cell Biol 114, 787–797.

Kreplak L, Bar H, Leterrier JF, Herrmann H, Aebi U (2005). Exploring the mechanical behavior of single intermediate filaments. J Mol Biol 354, 569–577.

Kreplak L, Herrmann H, Aebi U (2008). Tensile properties of single desmin intermediate filaments. Biophys J 94, 2790–2799.

Lariviere RC, Julien JP (2004). Functions of intermediate filaments in neuronal development and disease. J Neurobiol 58, 131–148.

Leduc C, Etienne-Manneville S (2017). Regulation of microtubule-associated motors drives intermediate filament network polarization. J Cell Biol 216, 1689–1703.

Lopez CG, Saldanha O, Huber K, Koster S (2016). Lateral association and elongation of vimentin intermediate filament proteins: a time-resolved light-scattering study. Proc Natl Acad Sci USA 113, 11152–11157.

Mucke N, Winheim S, Merlitz H, Buchholz J, Langowski J, Herrmann H (2016). In vitro assembly kinetics of cytoplasmic intermediate filaments: a correlative Monte Carlo simulation study. PLoS One 11, e0157451.

Mukai H, Toshimori M, Shibata H, Kitagawa M, Shimakawa M, Miyahara M, Sunakawa H, Ono Y (1996). PKN associates and phosphorylates the head-rod domain of neurofilament protein. J Biol Chem 271, 9816–9822.

Nakamura Y, Hashimoto R, Kashiwagi Y, Aimoto S, Fukusho E, Matsumoto N, Kudo T, Takeda M (2000). Major phosphorylation site (Ser^{55}) of neurofilament L by cyclic AMP-dependent protein kinase in rat primary neuronal culture. J Neurochem 74, 949–959.

Nowier RM, Friedman A, Brown A, Jung P (2023). The Role of neurofilament transport in the radial growth of myelinated axons. Mol Biol Cell, 34, 1–14.

Portet S, Leduc C, Etienne-Manneville S, Dallon J (2019). Deciphering the transport of elastic filaments by antagonistic motor proteins. Phys Rev E 99, 042414.

Preibisch S, Saalfeld S, Tomancak P (2009). Globally optimal stitching of tiled 3D microscopic image acquisitions. Bioinformatics 25, 1463–1465.

Rao MV, Campbell J, Yuan A, Kumar A, Gotow T, Uchiyama Y, Nixon RA (2003). The neurofilament middle molecular mass subunit carboxyl-terminal tail domains is essential for the radial growth and cytoskeletal architecture of axons but not for regulating neurofilament transport rate. J Cell Biol 163, 1021–1031.

Rao MV, Garcia ML, Miyazaki Y, Gotow T, Yuan A, Mattina S, Ward CM, Calcutt NA, Uchiyama Y, Nixon RA, Cleveland DW (2002). Gene replacement in mice reveals that the heavily phosphorylated tail of neurofilament heavy subunit does not affect axonal caliber or the transit of cargoes in slow axonal transport. J Cell Biol 158, 681–693.

Robert A, Tian P, Adam SA, Kittisopikul M, Jaqaman K, Goldman RD, Gelfand VI (2019). Kinesin-dependent transport of keratin filaments: a unified mechanism for intermediate filament transport. FASEB J 33, 388–399.

Roy S, Coffee P, Smith G, Liem RKH, Brady ST, Black MM (2000). Neurofilaments are transported rapidly but intermittently in axons: implications for slow axonal transport. J Neurosci 20, 6849–6861.

Sacher MG, Athlan ES, Mushynski WE (1992). Okadaic acid induces the rapid and reversible disruption of the neurofilament network in rat

dorsal root ganglion neurons. Biochem Biophys Res Commun 186, 524–530.
Sacher MG, Athlan ES, Mushynski WE (1994). Increased phosphorylation of the amino-terminal domain of the low molecular weight neurofilament subunit in okadaic acid-treated neurons. J Biol Chem 269, 18480–18484.
Saito T, Shima H, Osawa Y, Nagao M, Hemmings BA, Kishimoto T, Hisanaga S (1995). Neurofilament-associated protein phosphatase 2A: its possible role in preserving neurofilaments in filamentous states. Biochemistry 34, 7376–7384.
Sanchez I, Hassinger L, Sihag RK, Cleveland DW, Mohan P, Nixon RA (2000). Local control of neurofilament accumulation during radial growth of myelinating axons in vivo: selective role of site-specific phosphorylation. J Cell Biol 151, 1013–1024.
Sarria AJ, Nordeen SK, Evans RM (1990). Regulated expression of vimentin cDNA in cells in the presence and absence of a preexisting vimentin filament network. J Cell Biol 111, 553–565.
Schindelin J, Arganda-Carreras I, Frise E, Kaynig V, Longair M, Pietzsch T, Preibisch S, Rueden C, Saalfeld S, Schmid B, *et al*. (2012). Fiji: an open-source platform for biological-image analysis. Nat Methods 9, 676–682.
Sihag RK, Inagaki M, Yamaguchi T, Shea TB, Pant HC (2007). Role of phosphorylation on the structural dynamics and function of types III and IV intermediate filaments. Exp Cell Res 313, 2098–2109.
Sihag RK, Jaffe H, Nixon RA, Rong X (1999). Serine-23 is a major protein kinase A phosphorylation site on the amino-terminal head domain of the middle molecular mass subunit of neurofilament proteins. J Neurochem 72, 491–499.
Sihag RK, Jeng AY, Nixon RA (1988). Phosphorylation of neurofilament proteins by protein kinase C. FEBS Lett 233, 181–185.
Sihag RK, Nixon RA (1990). Phosphorylation of the amino-terminal head domain of the middle molecular mass 145-kDa subunit of neurofilaments. Evidence for regulation by second messenger-dependent protein kinases. J Biol Chem 265, 4166–4171.
Sihag RK, Nixon RA (1991). Identification of Ser-55 as a major protein kinase A phosphorylation site on the 70-kDa subunit of neurofilaments: early turnover during axonal transport. J Biol Chem 266, 18861–18867.
Stone EJ, Uchida A, Brown A (2019). Charcot-Marie-Tooth disease Type 2E/1F mutant neurofilament proteins assemble into neurofilaments. Cytoskeleton (Hoboken) 76, 423–439.
Strack S, Westphal RS, Colbran RJ, Ebner FF, Wadzinski BE (1997). Protein serine/threonine phosphatase 1 and 2A associate with and dephosphorylate neurofilaments. Mol Brain Res 49, 15–28.
Trimpin S, Mixon AE, Stapels MD, Kim MY, Spencer PS, Deinzer ML (2004). Identification of endogenous phosphorylation sites of bovine medium and low molecular weight neurofilament proteins by tandem mass spectrometry. Biochemistry 43, 2091–2105.
Uchida A, Alami NH, Brown A (2009). Tight functional coupling of kinesin-1A and dynein motors in the bidirectional transport of neurofilaments. Mol Biol Cell 20, 4997–5006.
Uchida A, Colakoglu G, Wang L, Monsma PC, Brown A (2013). Severing and end-to-end annealing of neurofilaments in neurons. Proc Natl Acad Sci USA 110, E2696–E2705.
Uchida A, Monsma PC, Fenn JD, Brown A (2016). Live-cell imaging of neurofilament transport in cultured neurons. Methods Cell Biol 131, 21–90.
Wang L, Brown A (2001). Rapid intermittent movement of axonal neurofilaments observed by fluorescence photobleaching. Mol Biol Cell 12, 3257–3267.
Wang L, Ho C-L, Sun D, Liem RKH, Brown A (2000). Rapid movement of axonal neurofilaments interrupted by prolonged pauses. Nat Cell Biol 2, 137–141.
Wickert U, Mucke N, Wedig T, Muller SA, Aebi U, Herrmann H (2005). Characterization of the in vitro co-assembly process of the intermediate filament proteins vimentin and desmin: mixed polymers at all stages of assembly. Eur J Cell Biol 84, 379–391.
Winheim S, Hieb AR, Silbermann M, Surmann EM, Wedig T, Herrmann H, Langowski J, Mucke N (2011). Deconstructing the late phase of vimentin assembly by total internal reflection fluorescence microscopy (TIRFM). PLoS One 6, e19202.
Xu Z, Tung VW (2001). Temporal and spatial variations in slow axonal transport velocity along peripheral motoneuron axons. Neuroscience 102, 193–200.
Yan Y, Brown A (2005). Neurofilament polymer transport in axons. J Neurosci 25, 7014–7021.
Yates DM, Manser C, De Vos KJ, Shaw CE, McLoughlin DM, Miller CC (2009). Neurofilament subunit (NFL) head domain phosphorylation regulates axonal transport of neurofilaments. Eur J Cell Biol 88, 193–202.
Yuan A, Nixon RA, Rao MV (2006). Deleting the phosphorylated tail domain of the neurofilament heavy subunit does not alter neurofilament transport rate in vivo. Neurosci Lett 393, 264–268.
Zhu Q, Couillard-Despres S, Julien J-P (1997). Delayed maturation of regenerating myelinated axons in mice lacking neurofilaments. Exp Neurol 148, 299–316.